Fast transport of water in carbon nanotubes
a review of current accomplishments and challenges

Sam, Alan; Hartkamp, Remco; Kumar Kannam, Sridhar; Babu, Jeetu S.; Sathian, Sarith P.; Daivis, Peter J.; Todd, B. D.

DOI
10.1080/08927022.2020.1782401

Publication date
2020

Document Version
Final published version

Published in
Molecular Simulation

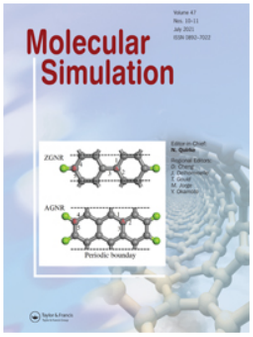

Molecular Simulation

ISSN: (Print) (Online) Journal homepage: https://www.tandfonline.com/loi/gmos20

Fast transport of water in carbon nanotubes: a review of current accomplishments and challenges

Alan Sam, Remco Hartkamp, Sridhar Kumar Kannam, Jeetu S. Babu, Sarith P. Sathian, Peter J. Daivis & B. D. Todd

To cite this article: Alan Sam, Remco Hartkamp, Sridhar Kumar Kannam, Jeetu S. Babu, Sarith P. Sathian, Peter J. Daivis & B. D. Todd (2021) Fast transport of water in carbon nanotubes: a review of current accomplishments and challenges, Molecular Simulation, 47:10-11, 905-924, DOI: 10.1080/08927022.2020.1782401

To link to this article: https://doi.org/10.1080/08927022.2020.1782401

MOLECULAR SIMULATION
2021, VOL. 47, NOS. 10–11, 905–924
https://doi.org/10.1080/08927022.2020.1782401

Taylor & Francis
Taylor & Francis Group

Fast transport of water in carbon nanotubes: a review of current accomplishments and challenges

Alan Sam [a], Remco Hartkamp [b], Sridhar Kumar Kannam [c], Jeetu S. Babu[d], Sarith P. Sathian [a], Peter J. Daivis [e] and B. D. Todd [f]

[a]Department of Applied Mechanics, Indian Institute of Technology Madras, Chennai, India; [b]Process and Energy Department, Delft University of Technology, Delft, The Netherlands; [c]Faculty of Science, Engineering and Technology, Swinburne University of Technology, Melbourne, Australia; [d]Department of Mechanical Engineering, Amrita Vishwa Vidyapeetham, Amritapuri, India; [e]School of Applied Sciences, RMIT University, Melbourne, Australia; [f]Department of Mathematics, Swinburne University of Technology, Melbourne, Australia

ABSTRACT

The intriguing mass transport properties of carbon nanotubes (CNTs) have received widespread attention, especially the rapid transport of water through CNTs due to their atomically smooth wall interiors. Extensive research has been dedicated to the comprehension of various aspects of water flow in contact with CNTs, the most prominent ones being the studies on slip and flow rates. Experimental and computational studies have confirmed an enhanced water flow rate through this graphitic nanoconfinement. However, a quantitative agreement has not yet been attained. These disparities coupled with incomplete knowledge of the mechanisms of water transport at nanoscale regimes are hindering the possibilities to integrate CNTs in numerous nanofluidic applications. In the present review, we focus on the slip and flow rates of water through CNTs and the factors influencing them. We discuss the key sources of discrepancies in water flow rate and suggest directions for future study.

ARTICLE HISTORY
Received 16 March 2020
Accepted 3 June 2020

KEYWORDS
Nanofluidics; carbon nanotube; water; friction coefficient; flow rate enhancement; slip length

1. Introduction

The advent of modern characterisation and nanoscale fabrication techniques have led to rapid developments in the field of nanoscience and technology [1]. The possibility of manipulating fluids, either by confining them in very small channels or by subjecting them to precisely controlled forces, is highly relevant in various fields of science and engineering, particularly in colloid science, membrane science and chemical engineering. The research efforts in this area have led to a drastic evolution in the field of nanofluidics [2,3], enabling it to carve its niche in the domain of nanoscience and technology. A decisive turning point in nanofluidics arose with the discovery of biological nanoscale channels such as aquaporins that were found to exhibit selective and controlled transport of ions and water across cell membranes [4,5]. This discovery inspired the development of artificial channels that could mimic the properties of biological nanopores [6,7]. The concept of artificial biochannels finds possible applications in the design of biosensors, lab-on-a-chip devices, desalination and artificial cells. Owing to their complex structure, it is difficult to study the intricacies of fluid movement through these biological nanoconfinements. This can be, however, studied by developing nanochannels with similar fluid behavioural properties but lacking their complexity. Research directed towards understanding the structural and dynamical properties of fluids confined to nanoscale channels has provided a major impetus to the field of nanofluidics.

At the nanoscale, surface effects become dominant owing to which the confined fluids start exhibiting unique physical, thermal, electrical and chemical characteristics that differ from the macroscale [8,9]. Various features of a nanochannel, such as its pore size, length, roughness and morphology, greatly influence the transport characteristics of the fluid [10–16]. Furthermore, new physical constraints are imposed on the fluid as the characteristic physical scaling lengths become comparable to the size of the flow domain, which can result in a further alteration in the behaviour of fluids in nanoconfinements. This behaviour can be exploited in the development of novel devices beneficial in blue energy harvesting, water desalination, hydrogen storage, drug delivery, etc. Also at the nanoscale, fluid flow is characterised by a velocity slip at the wall. The configuration and interaction of the fluid particles near the solid surface significantly influence the slip at the fluid–solid interface.

A major roadblock in conducting a scientific investigation in the nanofluidic regime is that existing continuum models fail to elucidate the experimental observations. As nanochannels comprise fewer molecules, there can be excessive molecular fluctuations and the fluid properties can become inhomogeneous [17]. This is especially true when the length scale of the confinement is of the same order of magnitude as the molecular size. Besides, interfacial layering of molecules results in locally varying state variables and transport coefficients, and anisotropic stresses. Furthermore, the very small length and time scales make experimental measurements of fluid flow through nanochannels challenging. It has long been realised that atomistic simulation methods like molecular dynamics (MD) can overcome these disadvantages and can be used to investigate the behaviour of nanoscale confined fluids.

Carbonaceous nanomaterials such as carbon nanotubes (CNTs) and graphene with their anomalous fluidic behaviour

CONTACT B. D. Todd btodd@swin.edu.au

promise a new era in the field of nanofluidics through enhanced functionality and by facilitating novel combinations of properties. The transport characteristics in CNTs exhibit a striking resemblance to aquaporins that enable them to emerge as a key material for studying molecular transport and nanofluidics. It has been found that the atomically smooth and hydrophobic surface of a CNT facilitates a rapid flow of water through its interior [18]. Despite tremendous advancement in the comprehension of physical mechanisms underlying fast water transport, there is still uncertainty about the use of CNTs in numerous practical applications. A major reason is the discrepancies among reported water flow rates, creating uncertainty in the field. The objective of this review is, therefore, to critically reflect on some of the promising findings from various experimental and computational studies on water flow in CNTs and discuss important sources for disparities in the flow rates reported amongst the studies. Research directed towards addressing the issues identified here may enable one to obtain a more precise way to measure or predict flow rates.

2. Carbon nanotube nanofluidics

CNTs may consist of one or more rolled sheets of graphene with a diameter ranging from sub-nanometres (<1 nm) to a few nanometres and length up to a few millimetres. The rolling direction can be specified by a chiral vector C perpendicular to the tube axis, defined by $C = na_1 + ma_2$, where a_1 and a_2 represent the unit cell vectors of the graphene sheets and the indices n and m describe the mapping orientation of carbon hexagons onto the nanotube. Depending on the value of the indices, the structure of the CNT can be categorised into three types: armchair (n=m), zigzag (m=0) and chiral ($m \neq n$), shown in Figure 1. The optical, mechanical and electronic properties of CNTs vary with each (n,m) combination.

Since their discovery by Sumio Iijima [20], carbon nanotubes have garnered the attention of researchers owing to their superior mechanical, chemical and electrical properties [21–23]. For example, the fast transport of water through CNTs has rendered them a potential candidate for various nanofluidic applications. The water flow rates in sub-nanometre CNTs are found to be almost equivalent to that of aquaporin [24–28].

Water is a unique fluid that exhibits anomalous properties in bulk as well as under confinement. The study of the structure and dynamics of nanoconfined water is an arena of great interest among researchers as it throws light upon challenging problems encountered in numerous applications such as nanomedicine, water purification, energy storage and conversion, as well as geophysical processes. In recent years, numerous experimental and MD studies have been performed to investigate the flow of water through CNTs. Although the idea that CNTs fill with water is somewhat counter-intuitive with regard to their hydrophobic nature, experimental evidence has proved it otherwise [29]. It has been observed that water fills the nanotubes spontaneously and also flows uninterruptedly with very small frictional losses [30–32]. Apart from the rapid water transport, characteristics such as high surface-area-to-volume ratio, high selectivity, ease of functionalisation and resistance to degradation make CNTs a suitable material for use in applications such as removal of metallic contaminants and biological impurities from water [33–35], nanofiltration [36–38] and sensing [39]. Of greater significance is their role in water desalination [40–43], wherein the rapid water transport provides a boost to the efficiency of membrane devices. The higher energy demand for water desalination and water purification with presently marketed commercial polymeric membranes translates into higher operating costs [44–46]. More efficient water treatment devices can be attained by synthesising highly permeable membranes with selective solute rejection properties. This would reduce energy consumption and thus the total cost of water treatment [47–49]. The flow rate of water was found to be enhanced by 10 times in a CNT-based polymer membrane compared to the pure polymer membrane. Functionalising pores of well-defined diameters can be used to achieve selective rejection of ions or organic solutes [50], thus creating the desired membrane properties for water treatment applications. The future perspective includes the coupling of fluidics and electronics to create CNT-based circuits with selective functional gates that can manipulate molecular and ionic transport with enhanced control for various nanofluidic applications.

3. Entry and fast transport of water in CNTs

The pioneering studies on the interaction between water and hydrophobic CNT channels were based on molecular dynamics simulations [24,51–56]. A flow rate of 51×10^{-14} cm^3/s was predicted in a CNT of 0.81 nm diameter [24] which is 2–3 orders of magnitude higher when compared to the flow rate calculated with the classical Hagen–Poiseuille equation. This ratio of measured flow rate (from experiments or atomistic simulations) to the expected flow rate calculated based on the continuum formalism is defined as the flow rate enhancement. The flow rate enhancement is a critical parameter to be monitored for the use of these graphitic conduits in various nanofluidic applications. The computationally observed high conduction of water through CNTs was later verified experimentally [29]. However, the simulated magnitude of the flow enhancement did not agree with experiments.

There have been numerous simulation studies that discuss the possible reasons for the entry of water in such hydrophobic channels and the subsequent high flow rate [24,57]. In their pioneering work Hummer et al. [24] found that when the CNTs become extremely narrow (<1 nm), water molecules form a one-dimensional single-file network rather than a tetrahedral network (in the bulk state). Thus the average number of hydrogen bonds per water molecule inside the CNTs is reduced from approximately 3.5 [58–60], to a maximum of two in narrow CNTs [24,32,61,62]. The single-file filling of water molecules was later experimentally observed by Cambré et al. [63] using resonant Raman scattering for CNTs with diameter reduced even down to 0.55 nm. In tubes of single-file configuration, the highly oriented water molecules can rotate freely along the aligned direction causing additional rotational entropy, which partially compensates the loss of energy due to the reduction in the average number of hydrogen bonds. Despite the loss of hydrogen bonding and weak water-CNT attraction, the lower excess chemical potential of water inside

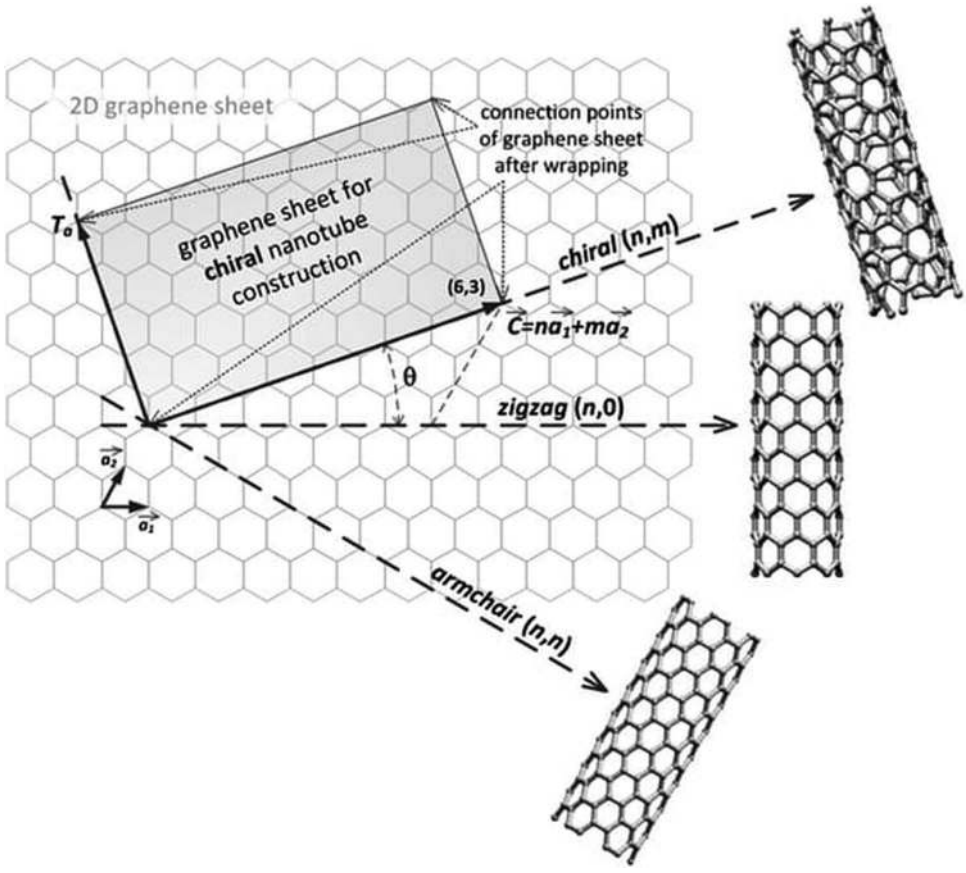

Figure 1. A sheet of graphene rolled to show the formation of different types of single walled carbon nanotube. Republished with permission of Royal Society of Chemistry from Prasek et al. [19]; permission conveyed through Copyright Clearance Center, Inc.

the tubes enables the continuous filling of CNTs with water from the surrounding reservoir.

In CNTs of diameter ranging from 1 to 2.7 nm, water adopts inhomogeneous arrangements with the molecules forming concentric layers, shown in Figure 2. In addition to the formation of inhomogeneous fluid layers inside CNTs, the repulsion of the water molecules by the nanotube walls and attraction to each other as a consequence of hydrophobicity leads to very high flow rates [65]. The hydrophobicity of the atomically smooth wall surface causes a low-density depletion region (<5% concentration of bulk water) between the tube wall and water molecules. The 'free' OH bonds (dangling bonds) in the depletion region near the surface form weak hydrogen bonds between adjacent water molecules at the hydrophobic CNT surface, resulting in fast conduction of water through the tube. However, the hydrophobic contributions of the tube can be maximally utilised in CNTs (<1 nm) where the water molecules form an unstable hydrogen-bonded network [66].

The diameter-dependent molecular arrangements and the associated hydrogen bonding significantly alter the water transport characteristics in confinements of sub-nanometre dimensions. In larger pores, with diameters exceeding 10 times the molecular diameter (>2.7 nm), water forms disordered bulk structures at the centre as in macroscale flow domains. Despite this bulk-like structure, the molecules still exhibit higher velocities than calculated based on the continuum formalism. This can be attributed to the dynamics of water at the CNT surface, where the solid/fluid friction coefficient was found to be very low, leading to a high slippage of water. The friction coefficient was observed to be dependent on the tube diameter, with negligibly small friction in very narrow channels. The diameter-dependency of the friction coefficient arises due to the smoothening of the potential energy landscape felt by water molecules upon their transmission, shown in Figure 3. An increase in the curvature (or decreasing diameter) leads to a decrease in the corrugation of the energy landscape, such that the resistance offered by the CNT surface to the transmission of water declines. Thus the continuous and rapid transport of water through the sub-nanometre diameter channels is credited to the lower potential energy barrier, unique orientations and the durable strong hydrogen bond networks. With an increase in tube diameter, the effects of curvature and confinement decrease with a simultaneous increase in friction coefficient, until it reaches a maximum value equivalent to that of the planar graphene channel. This increase in the interfacial friction coefficient leads to a decrease in the flow enhancement [30].

Another major parameter that has been used to investigate the flow behaviour of confined fluids is the slip length. The amount of slip at the interface between a fluid and a solid surface can be quantified by the slip length (L_s), defined as the distance from the wall at which the fluid boundary slip velocity (u_s) equals the wall velocity, see Figure 4. The mathematical

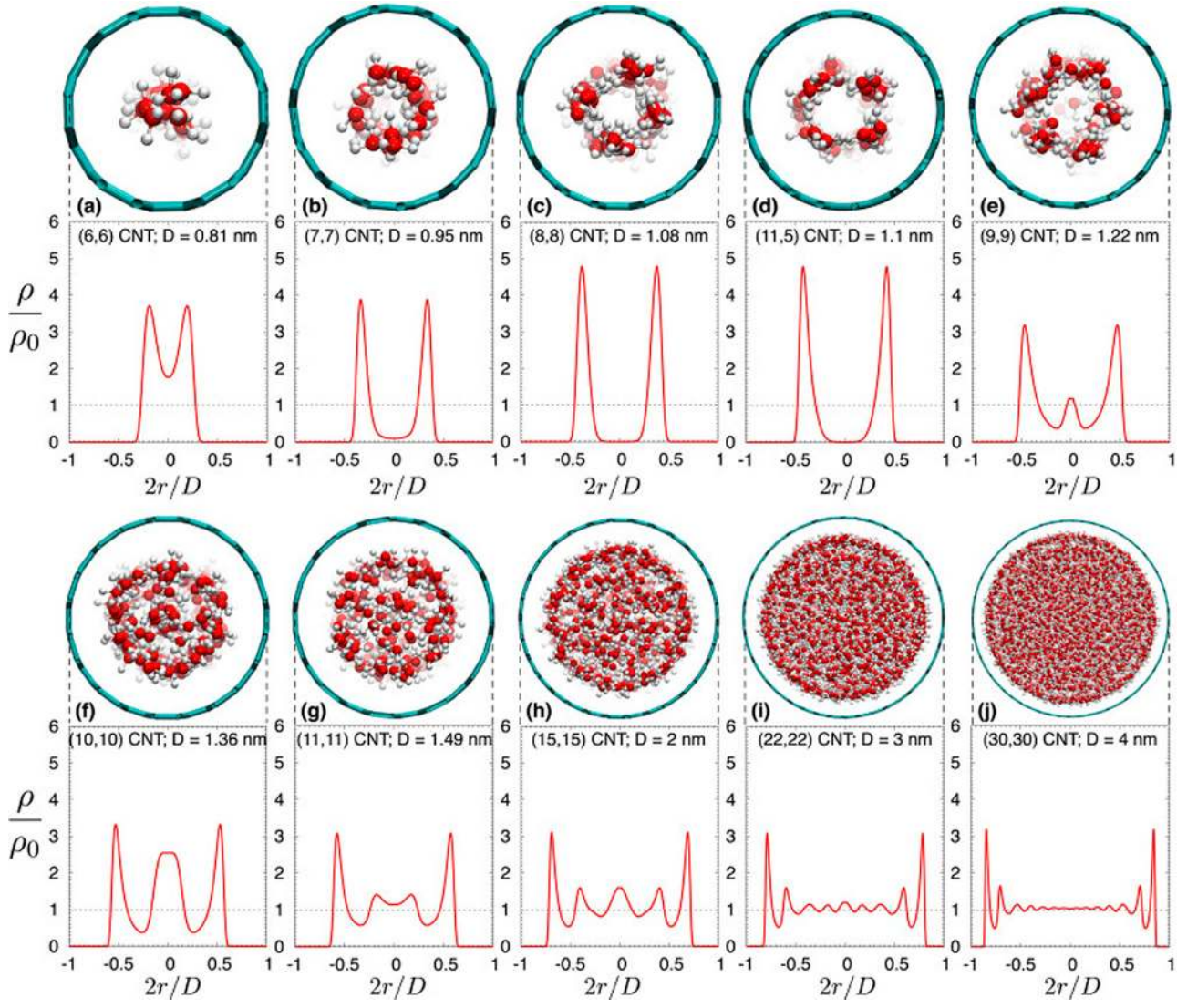

Figure 2. (Colour online) Cross-sectional view of water inside CNTs with different diameters. Normalised radial density profiles are also shown. Reprinted after Borg et al. [64].

definition for slip length was determined by Navier [68] where the slip behaviour is characterised by

$$L_s = \frac{\eta}{\lambda}. \tag{1}$$

Here η is the fluid shear viscosity and λ is the interfacial friction coefficient at the fluid–solid interface. An alternate expression to calculate L_s and its relationship with the flow rate enhancement (ε) is given by Equations (2) and (3),

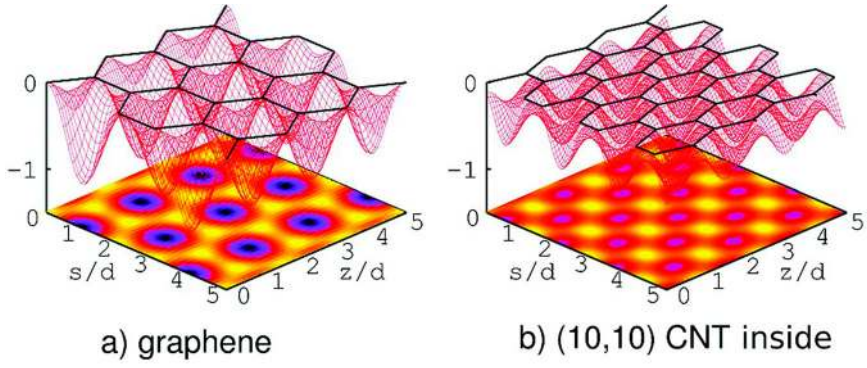

Figure 3. (Colour online) Curvature effects on the interaction energy landscape felt by a single water molecule in the first layer close to the carbon structure, computed from a direct summation of the water–carbon interaction at a distance σ from the carbon structure. The potential (calculated in kJ/mol) inside a curved CNT exhibits both a structural change and a smoothing of the potential wells. Reprinted with permission from Falk et al. [30]. Copyright (2010) American Chemical Society.

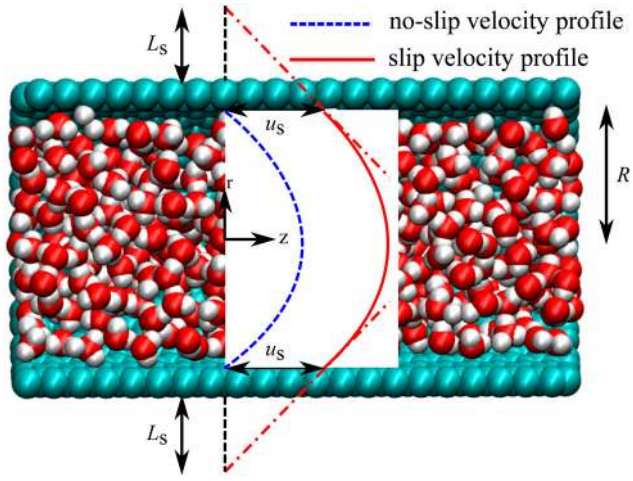

Figure 4. (Colour online) Schematic depiction of velocity profiles of water flow through carbon nanotubes with and without boundary slip. L_s characterises the fluid–solid interfacial slip. Republished with permission of Royal Society of Chemistry from Sam et al. [67]; permission conveyed through Copyright Clearance Center, Inc.

respectively.

$$u_s = u(R) = L_s \left.\frac{\partial u(r)}{\partial r}\right|_{r=R} \tag{2}$$

$$\epsilon = \frac{Q_{slip}}{Q_{no-slip}} = \left(1 + \frac{8L_s}{D}\right) \tag{3}$$

Here Q_{slip} is the observed flow rate, $Q_{no-slip}$ is the expected flow rate calculated from the Hagen–Poiseuille equation (assuming the no-slip boundary condition), and D is the diameter of the tube. L_s is negligible relative to the flow domain size in macroscale channels but becomes significant as the channel size decreases to a few molecular diameters. The slip length and slip velocity of flow through a tube are closely related to the hydrophobicity of the wall, the tube diameters and the driving force acting on the fluid. Hydrophobicity causes lower interfacial friction, leading to large slip length and slip velocity, thereby increasing the flow rate. The slip velocity and the curvature of the velocity profile both scale with the driving force in the linear regime, such that the slip length remains constant in this regime. The velocity profile maintains its parabolic shape, but the large slip lengths and the small variations in the velocity profile across the tube diameter make the velocity profile appear somewhat plug-like, shown in Figure 5.

Due to their high surface-to-volume ratio, the flow through nanochannels strongly depends on the nature of the solid–liquid interface. For example, slip lengths of water in hydrophobic carbon nanostructures, such as graphene slit pores and CNTs, greatly exceed typical pore dimensions [11–13,24,29,30,40,70–76]. Much smaller slip lengths are typically observed in less hydrophobic environments, such as boron nitride nanopores [76,77]. In addition to the influence of the material, L_s also shows a dependency on the channel geometry. For example, in cylindrical nanopores, L_s varies with the tube diameter due to the effect of curvature [11,13]. However, as mentioned above, curvature and confinement effects diminish

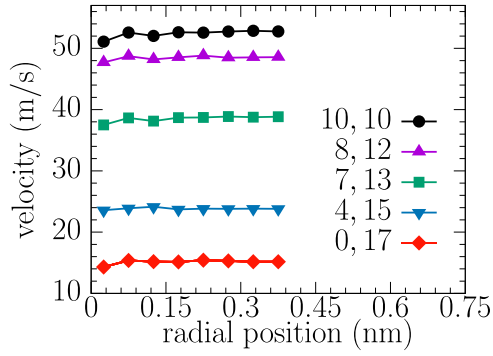

Figure 5. (Colour online) Plug-like velocity profiles of water in carbon nanotubes (CNTs) of different chiralities. Reproduced from Sam et al. [69] with permission from the PCCP Owner Societies.

upon increasing the tube diameter, such that L_s converges towards values corresponding to a slit pore, for which the slip length is independent of the pore width [30,75]. Although understanding and predicting slip in nanochannels is pivotal for the development of nanofluidic devices, measurements and simulations have thus far not been able to provide a consistent view of the amount of slip at given surfaces. Slip lengths of 1–50,000 nm have been reported for CNTs of 0.8–10 nm in diameter. It is thus paramount to be able to accurately predict the slip between water and CNTs to design optimised devices for nanofluidic applications such as water desalination, blue energy harvesting and drug delivery [78].

4. Studies on water flow through CNTs

Since membranes were contemplated to be the most effective way to incorporate CNTs in industrial-scale mass transport applications, a major proportion of experimental studies utilised CNT encapsulation in membrane matrices. Various spectroscopic techniques such as Transmission Electron Microscopy (TEM), Scanning Electron Microscopy (SEM), Atomic-force Microscopy (AFM), X-ray diffraction and so on have been employed for the characterisation of the CNT membrane. Experimentally, it is possible to measure the flow rates and slip length but explaining the physical mechanisms of rapid water transport in nanochannels is rather difficult. Molecular simulations provide detailed insight into mechanisms of water transport in these sub-nanometre channels from a molecular perspective. Experimental and computational studies, as well as the continuum based theoretical approaches for explaining flow rate enhancement, are discussed in detail in the following sections.

4.1. Experimental studies

The functionality of CNTs for various nanofluidic transport applications is greatly influenced by their structure and orientations in the membrane matrix [19]. The preliminary step in experimental investigations of the transport phenomena of water inside CNTs begins with the synthesis of finely controlled structures of CNTs, either aligned or randomly oriented. The fabrication methods like electric arc discharge [79–87], laser ablation [88–91] and chemical vapour deposition (CVD)

[92–100] enable the production of CNTs from small to large scales. Membranes with aligned CNTs are found more suitable for applications involving fluid transport [101,102].

Catalytic CVD is the most efficient and well-established method to produce a forest of high-quality vertically aligned CNTs (VA-CNTs). This method has superior control over the lateral and longitudinal dimensions, alignment, orientation and purity. The method utilises carbon atoms from vapours of hydrocarbons, such as methane, ethylene or acetylene, to supply the growth of the CNTs. The carbon source gas flows on a quartz substrate, patterned with the compactly packed catalyst (by spin coating) such as cobalt, nickel or iron at a high temperature (~900°C), which acts as a nucleation site for the growth of the nanotube. The carbon atoms are supersaturated to form aligned CNTs on the quartz substrate. The size of the metallic catalyst is critical to the diameter of the obtained nanotubes [103,104]. Single or double-walled nanotubes can be produced only when the size of the catalyst particles is restricted to sub-nanometre dimensions. The aligned tubes are then embedded in an impermeable matrix, either a polymer (polysulfone, polystyrene, epoxy, parylene) or an inorganic material (silicon nitride), to form a composite film [40,105,106]. The tube endings appear closed initially due to the formation of unrestrained layers at their ends owing to spin coating. Plasma etching opens up the tube endings. Plasma oxidation not only assists in the removal of catalyst impurities and excess polymers on the surface of the composite film but also aids in the introduction of functional groups at the tips of the open-ended CNTs. CNTs of diameters in the range of 1–100 nm and length up to a few micrometres can be manufactured with this technique [103,106]. Compared to randomly oriented CNTs, an added advantage of VA-CNTs is the ease of functionalisation of the pore endings or core. However, the laborious and complex processes involved in the fabrication of VA-CNTs and also the lack of reliable procedures in producing highly dense CNT pores of uniform sub-nanometre lateral dimensions makes its utility for commercial purposes highly challenging.

Pressure-driven flow of water through a CNT membrane was first experimentally studied by Majumder et al. [29]. They estimated the average CNT diameter for water transport to be 7 nm by assessing the ion permeability of the membrane. For a pressure range of 0.7–1.0 bar, a slip length of 3–70 m and a flow enhancement of $4-6 \times 10^4$ was obtained. The flow velocities for the pressure ranges were 10–44 cm/s, which was 4–5 orders of magnitude higher than predicted by the Hagen–Poiseuille equation. The high transport rates were attributed to slip at the CNT walls. To probe the chemical selectivity of the CNT membrane, the effect of functionalisation of surface and tips of the nanotubes on the flow rate enhancement was investigated [107]. A gradual hydrophilic functionalisation of CNT membranes was found to reduce the flow enhancement from 5×10^4 (as-produced) to 2×10^2 for the tip-functionalised tubes. An even smaller enhancement factor (less than 5) was obtained when the core and tip of the tubes were both functionalised, implying a disruption of the slip boundary conditions.

Du et al. [71] devised a method to produce superlong vertically aligned carbon nanotubes (SLVA-CNTs) of the length scale of millimetres, with relatively large surface areas that facilitated its integration into various nanosized devices. Water was driven through all the SLVA-CNTs in a 2 cm × 2cm nanotube membrane at pressures 1 and 2 atms. A flow rate of 4.7×10^{-20} m^3/s and velocity of 6×10^{-4} m/s was obtained for a double-walled CNT of diameter 10 nm at ambient pressure whereas a pressure of 2 atm resulted in a flow rate of 2.6×10^{-18} m^3/s and a velocity of 3.4×10^{-2} m/s respectively. Holt et al. [40] fabricated double-walled CNTs of sub-nanometre dimensions (1.3–2 nm) on the surface of a silicon chip. The measured flow rates exceeded the expected ones by 3–4 orders of magnitude (1500–8400) and the slip length was between 380 and 1400 nm.

Contrary to the previous experiments, where the average CNT diameter was less than 10 nm, Whitby et al. [108] considered a larger scale regime (10–100 nm) to look into the water flow characteristics and also to examine whether flow rate enhancement can be achieved at these ranges. Whereas in the conventional CVD technique, CNTs were grown on metallic catalyst particles, here ethylene vapour (carbon source) was passed onto the porous surface of an aluminium oxide template at 675°C. This resulted in the deposition of carbon layers on the porous template forming CNT arrays of pore density $\sim 1.07 \times 10^{10}$ pores/cm^2. The average diameter of the carbon nanopores was found to be ~44 nm. Fluid flow was driven by maintaining a hydrostatic pressure difference with the help of a syringe pump and the flow rate was determined by periodically weighing the water that emerged out from the array. Even though the water flow rate exceeded predictions from the no-slip Poiseuille relation by 1 order of magnitude (22–34), the flow rate enhancement shows a drastic reduction with the increase in diameter of CNTs. From this enhancement data, the slip length was calculated to be between 113 nm and 177 nm.

Qin et al. [70] utilised a field-effect transistor (FETs) array-based design to directly calculate the flow rate of water through individual ultralong carbon nanotubes. The setup consisted of three FETs in series made on an individual CNT of length 6 μm and diameter ranging between 0.81 and 1.59 nm, shown in Figure 6. The average flow velocity was calculated after monitoring the time taken for water to reach from one FET to the next. With the decreasing diameter of the tubes considered for the investigation, the flow velocity values were obtained between 46 and 928 μm/s. The corresponding slip

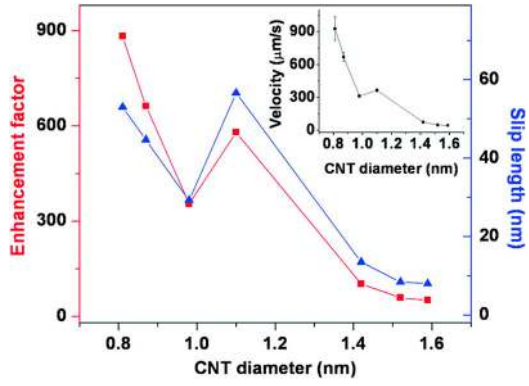

Figure 6. (Colour online) Slip length and flow enhancement as a function of tube diameter are shown. Reprinted with permission from Qin et al. [70]. Copyright (2011) American Chemical Society.

length and flow rate enhancement range between 8–53 nm and 51–882 respectively. A discontinuity observed in the enhancement factor in the diameter ranges of 0.98–1.10 nm was attributed to transition from the continuum to sub-continuum regimes.

In a recent experimental study, Secchi et al. [76] developed a novel method to estimate the fluid flow rate in nanochannels accurately and observed that the slip length of water in CNTs increases monotonically with a decrease in tube diameter. When compared to the no-slip Hagen–Poiseuille formalism, the water flow rate was enhanced nearly by a factor of 24 in a CNT of diameter 30 nm. The other intriguing finding was that, for similar diameters, the slip length in a CNT was approximately 10^2 times higher than in a boron nitride nanotube (BNNT). The differing flow rates in CNT and BNNT despite their geometrical similarities were attributed to the difference in the electronic properties of both materials.

4.2. Simulations

Molecular dynamics simulations have emerged as a powerful tool to study the physical behaviour of fluids by modelling the motion and interactions of atoms and molecules. The application of MD simulations to nanofluidics is highly efficacious in providing a detailed understanding of molecular and ionic transport in nanoconfinements owing to the accurate control of conditions and a high spatial and temporal resolution, beyond what is typically obtainable in laboratory experiments. With an increase in the availability and capabilities of supercomputers as well as a drastic improvement in the techniques, methods and algorithms, the future of molecular dynamics is highly promising as it facilitates the extraction of useful information from even highly complex problems of the physical world.

MD simulations of flow through pores can be utilised for studies in which either an infinitely long pore or a finite pore is modelled. The former makes use of a tube or a porous material filled with fluid and placed in a periodic simulation cell. An infinitely long tube is a realistic model for CNTs, owing to their very large aspect ratios. It is also advantageous in that a fully developed flow can be studied without the entrance/exit effects, which in turn facilitates in generating information about the slip lengths or local fluid properties across the tube diameter. For a finite pore model, the effects at the entrance/exit on mass flow rate through the pore and rejection of the accompanying solutes are studied. Figure 7 is a schematic of a simulation setup showing a finite CNT with graphene sheets at its ends, connecting two water reservoirs. The fluid pressure in this system can be controlled by regulating the volume of the bulk reservoirs. However, in finite models, the pore entry effects extend far beyond the entrance region, necessitating a long tube for attaining fully developed flow. This incurs greater computational expense. Both systems mentioned above have been widely used in MD simulations for deciphering the mechanisms underlying fast water transport in CNTs. The key factors that influence the enhanced flow rates are discussed below.

Hummer et al. [24] performed one of the first simulation studies on the flow of water through a CNT to gain insight into how fluid transport under the graphitic nanoconfinement deviates from flow through macro channels. Here, MD simulations were performed on an armchair CNT (6,6) having a diameter 0.81 nm and length 1.34 nm immersed in a water reservoir. Water was found to spontaneously fill the CNTs irrespective of their hydrophobicity. Rather than forming a tetrahedral bulk structure, a one-dimensional water chain was formed that can freely rotate about its aligned direction. Figure 8(a) shows the probability distribution of the binding energy of water molecules in bulk and CNT confinement. From the figure, it can be understood that the binding energy distribution of water molecules under CNT confinement is narrower and the weakly bound states are less populated (tilted arrows), whereas, in bulk flow, the distribution is found to be Gaussian in nature. Correspondingly, the lower excess chemical potential of water inside CNTs compared to the bulk water (shown in Figure 8b) also compensates for the energy loss resulting from the reduction in hydrogen bonds, facilitating a continuous water flow through CNTs. Flow rate obtained at 1 bar pressure and 300 K was 51×10^{-14} cm^3/s, which is comparable to flow in aquaporin protein channels. The rapid water conduction can be attributed to the smooth hydrophobic CNT walls that result in strong repulsion between the water file and the channel wall. However, hydration of the CNT was strongly affected by even a minor reduction in the carbon-water interaction parameters (i.e. increased hydrophobicity), showing a transition from the filled to the empty states within nanoseconds. We note here that applying large perpendicular electric fields has been shown to adversely affect water permeation by causing a disruption of the single-file structure [109].

Thomas et al. [12] analysed the influence of local variations in structural and thermophysical properties of confined water

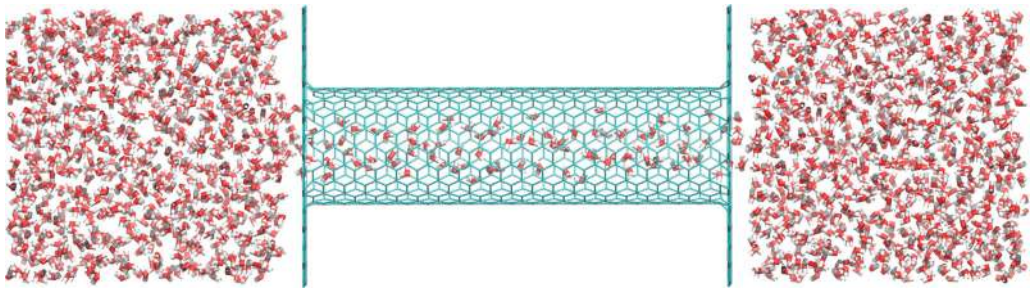

Figure 7. (Colour online) Typical simulation system with two water reservoirs connected by a CNT.

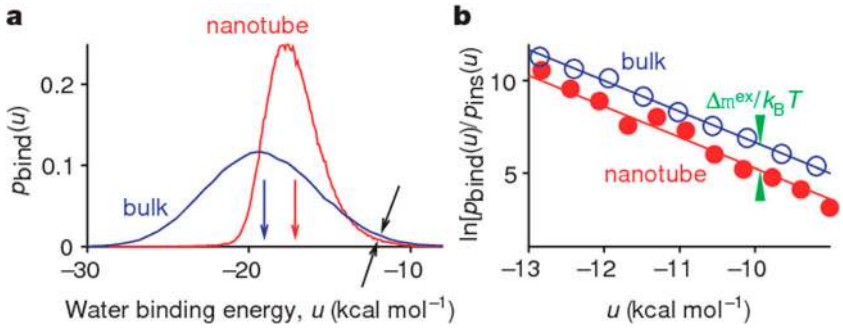

Figure 8. (Colour online) (a) Probability distribution of binding energies for bulk water (blue) and water inside the nanotube (red). Vertical arrows indicate average binding energies. Tilted black arrows indicate the cross-over region, in which weakly bound states are more populated in bulk water. (b) The vertical distance between the parallel lines of slope gives the difference in the excess chemical potential between bulk and CNT confinement. Reprinted with permission from Hummer et al. [24]. Copyright (2001) Springer Nature.

on flow enhancement. A comparison of flow in CNTs with diameters ranging from 1.66 to 4.99 nm was performed. Water was driven by gravitation-like acceleration or by utilising a piston to bring about a pressure gradient across the system length. The radial velocities were predicted directly from the simulations by following the trajectory of each particle. The average flow velocities obtained were in the range of 3–14 m/s. It was inferred that for a particular diameter of CNT, the volumetric flow rate calculated by integrating the radial velocity profiles bears a linear relationship with pressure gradient while for a fixed pressure gradient, the volumetric flow rate increases with increasing diameter of the CNTs. A monotonically decreasing flow enhancement factor with an increase in diameter was established from the simulations. The axial self-diffusion coefficient (D_z) predicted from the velocity autocorrelation functions (Green–Kubo relation) in equilibrium molecular dynamics (EMD) was used to evaluate the effective viscosity of water in nanoconfinements using the Einstein relation, as given in Equation (5).

$$D_z = \frac{1}{N}\sum_{i=0}^{N}\int_0^{\infty}\langle u(t)\cdot u(0)\rangle \mathrm{d}t \tag{4}$$

$$\eta = \frac{k_B T}{3\pi a}\frac{1}{D_z}. \tag{5}$$

Here $u(t)$ is the centre of mass velocity of molecule i and a is the hydrodynamic diameter of the fluid molecule. The viscosity of water increased with the tube diameter, gradually approaching the bulk value, shown in Figure 9. A decreasing slip length with the increasing cross-sectional area was also obtained which eventually reaches a value of 30 nm for all the CNTs with a diameter greater than 5 nm, equivalent to the slip length obtained for planar graphene channels using the same

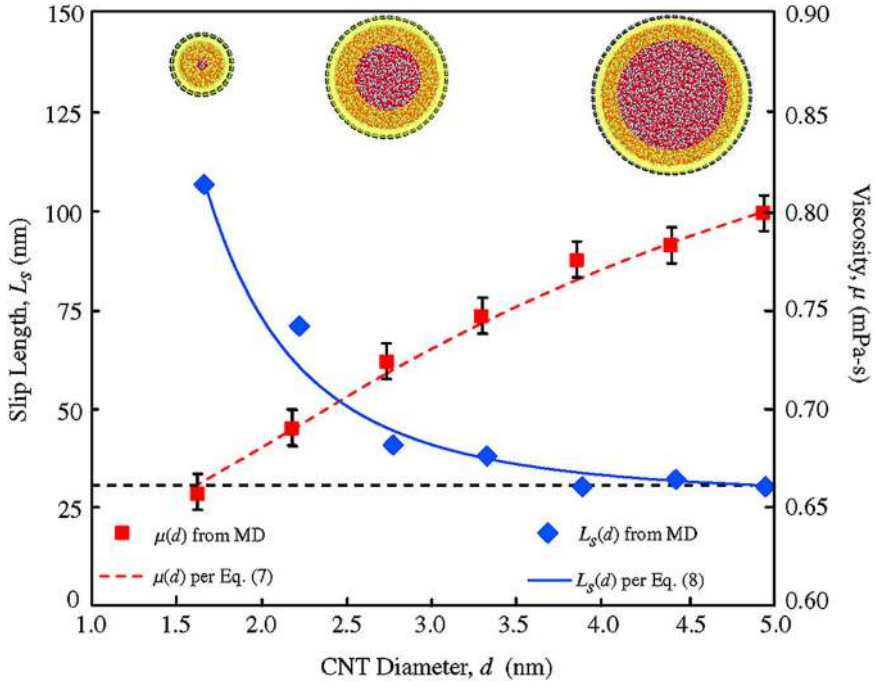

Figure 9. (Colour online) Slip length and viscosity of water as a function of CNT diameter. Reprinted with permission from Thomas et al. [12]. Copyright (2008) American Chemical Society.

simulation methodology. The increase in the flow rate enhancement factor with reducing CNT diameter was attributed to the decreasing viscosity of water and increasing slip length at the nanotube surface.

For CNT diameters between 0.83 and 1.66 nm [13], the average flow velocity was found to vary non-linearly with the CNT diameter while keeping the pressure gradient constant. Since the structures formed by water molecules in very narrow tubes (<1.6 nm) differ greatly from the tetrahedral structures in bulk water, the flow rate enhancement in such CNTs cannot be explained in the standard continuum framework (even with slip boundary condition). The flow rate enhancement increases monotonically with decreasing diameter down to 1.39 nm but exhibits an abrupt decline once the diameter is further reduced to 1.25 nm as a result of the change in the molecular configurations of water from a disordered structure to stacked hexagons. The axial distribution functions demonstrated a high correlation in the positions and movements of the water molecules in smaller CNTs, indicating a collective motion. A concurrent change to the single-file structure was observed when the diameter was reduced to 0.83 nm. It was concluded that the confinement-induced structural ordering impacts the sub-continuum water transport and flow-rate enhancement.

The variation in viscosity of water inside CNTs with diameters ranging from 0.81 to 5.42 nm was later confirmed by Babu and Sathian [74]. They proposed a theoretical method based on the Eyring theory of reaction rates to calculate the water viscosity in nanoconfinements. The viscosity was found to increase nonlinearly with the tube diameter. In CNTs of very small diameters (<2 nm), the viscosity was almost negligible and the structural configurations were very different from those of the bulk water. Due to the reduced viscosity, the activation energy required to initiate flow was considerably smaller, causing an enhanced flow rate in nanopores.

A more profound understanding of the elevated flow rates in CNTs was achieved by Falk et al. [30], who studied the effects of curvature and confinement on the friction between water and various carbon-based surfaces, shown in Figure 10. Friction coefficients were calculated from equilibrium and non-equilibrium MD (NEMD) simulations in the following systems: (a) CNTs with water flowing inside, (b) CNTs with water flowing outside and (c) water flowing in between two graphene sheets, where the diameter of the CNTs was varied from 0.68 to 20.4 nm and the width of the slit pore from 0.68 to 6.11 nm. In NEMD, an acceleration of 10^{-4} nm/ps^2 (equivalent to a pressure gradient of 10^{14} Pa/m) was given to all the water molecules for the flow to occur. The friction coefficients, calculated from EMD (Green–Kubo relations) and NEMD (ratio of the friction force of water at the surface to the slip velocity), showed similar trends, i.e. increased friction coefficient with an increase in diameter for water inside CNTs, whereas friction coefficient decreases with diameter for water outside the tubes. A low friction coefficient causes a large flow rate enhancement of water through very narrow CNTs. The rapid water transport in small confinements has been attributed to the smoothened corrugations of the energy landscape felt by water. The single-file water structure formed inside the extremely narrow CNTs affects the reduction in friction coefficient and facilitates faster transport. However, there was no correlation between the structure of water and the confinements for CNT diameters greater than 1.6 nm. The slip length was then predicted from the friction coefficient as in Equation (1). Corresponding to an increase in diameter from 1 to 7 nm, the slip length showed a monotonic decrease from 500 to 120 nm, respectively. However, in graphene sheets a constant slip length (80 nm) and friction coefficient were observed irrespective of the varying confinement size, confirming that the friction in CNTs is induced by the tube curvature.

Since friction of water at the tube walls is negligibly small in narrow CNTs, slip length predicted from the resulting streaming velocity profiles in NEMD simulations (Equation 2) could lead to unreliable estimates. Using the EMD method proposed by Hansen et al. [110], Kannam et al. [75] calculated the interfacial friction coefficient to predict slip length [68] (as in Equation 1) in CNTs of diameters varying from 1.62 to 6.5 nm. The results obtained from the EMD method were compared to those obtained from NEMD simulations. In NEMD, Poiseuille flow of water in CNTs was generated by applying a gravity-like external acceleration to the water. The velocity profiles were plug-like with high slip velocities and the profiles were fitted to a quadratic equation ($u = ar^2 + b$). The parameters a and b were constrained such that it should satisfy the shear viscosity of bulk water. All the results obtained from EMD and NEMD methods were in excellent agreement,

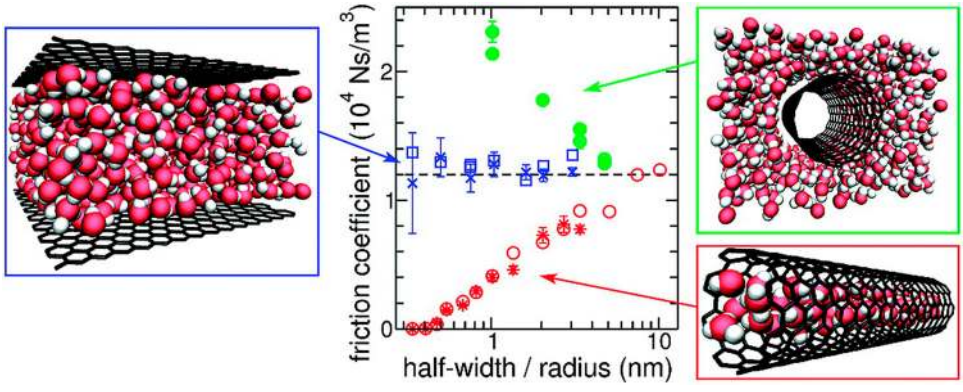

Figure 10. (Colour online) Flow of water inside CNT, outside CNT and between graphene sheets. Friction coefficient with the confinement R, for water inside/outside CNT (with a diameter $d = 2R$) and between graphene sheets (at a distance H=2R) are shown. Reprinted with permission from Falk et al. [30]. Copyright (2010) American Chemical Society.

with the slip lengths ranging from 180 to 75 nm and the flow enhancement from 870 to 90 for the smallest to highest diameter CNTs. For wider tubes, the slip length of water in CNTs reached approximately to that in graphene (60 nm), implying a decrease in the confinement and curvature effects.

Concerning the large surface effects in nanoconfinements, the slippage of the confined fluid depends significantly on the nature of the interacting solid. Joseph et al. [73] studied the flow velocity and structure of water adjacent to the tube surface in four systems; (a) CNT with a bond length of 0.142 nm, (b) boron nitride nanotube (BNNT) with a bond length of 0.144 nm, (c) a nanotube with higher attractive Lennard–Jones interaction parameters of silicon (NT with Si LJ) and (d) a nanotube with hexagonal unit cell consisting of three rings each of (16,16) and (18,18) CNT, which is rough compared to the other three nanotubes. All the nanotubes have a similar diameter (1.6 nm). The velocity profile was plug-like along the tube radius in all the smooth systems due to the large slip at the solid boundary. However, a variation in velocities was observed among the systems, with CNT showing the highest value, followed by BNNT, NT with Si LJ and rough nanotube the lowest. At the interface between the wall and water molecules, a velocity 'jump' was found to occur in all the smooth NTs, shown in Figure 11. The velocity 'jumps' reduced with the increase in the concentration of water in the immediate layer next to the smooth surface. The region of low water concentration (or density) found adjacent to the walls where the velocity 'jumps' takes place is defined as the depletion region. The mass flow rate was calculated from the concentration and velocity profiles of water and the flow enhancement was then calculated by comparing the predicted flow rate with the flow rate determined by using the Hagen–Poiseuille equation. The results show the highest flow enhancement for the CNT, followed by the BNNT, NT with Si LJ, and the lowest in rough tubes. This larger flow rate enhancement inside the CNTs compared to the other nanotubes has been attributed to the considerable number of free O–H bonds or dangling bonds in the depletion region, thereby weakening the hydrogen bonding between adjacent water molecules at the hydrophobic CNT surface.

A recent study by Sam et al. [69] demonstrated the effects of chirality of a carbon nanotube (CNT) on water transport. The tube with armchair configuration showed the highest flow rate, followed by chiral and then zigzag tubes of similar diameter. The large dependency of water flow on the tube chirality was explained by the variation in interfacial friction coefficient, wherein the force experienced by a water molecule along the axial direction of the tube increases with the change in CNT type from armchair to chiral and then to the zigzag structure. The force landscape of a single water molecule on armchair CNTs revealed larger regions of minimal force that provide favourable pathways for water movement. The extent of these minimal force regions reduced as the structure varied to chiral and reached a minimum for zigzag configurations. Using molecular mechanics calculations of the potential energy surface, Liu et al. [111] also attributed the altered diffusion coefficient of water in armchair and zigzag tubes to the different paths for water movement along the CNT surface.

Selectivity is an aspired characteristic of CNTs for incorporating it into various nanofluidic transport applications. The majority of MD studies have considered the surface of CNTs to be non-polar. Majumder and Corry [42] simulated CNTs to get an insight into the fluid flow rate variations corresponding to different surface charges (polar CNTs) and compared the results with their previously conducted experiments. Polar and

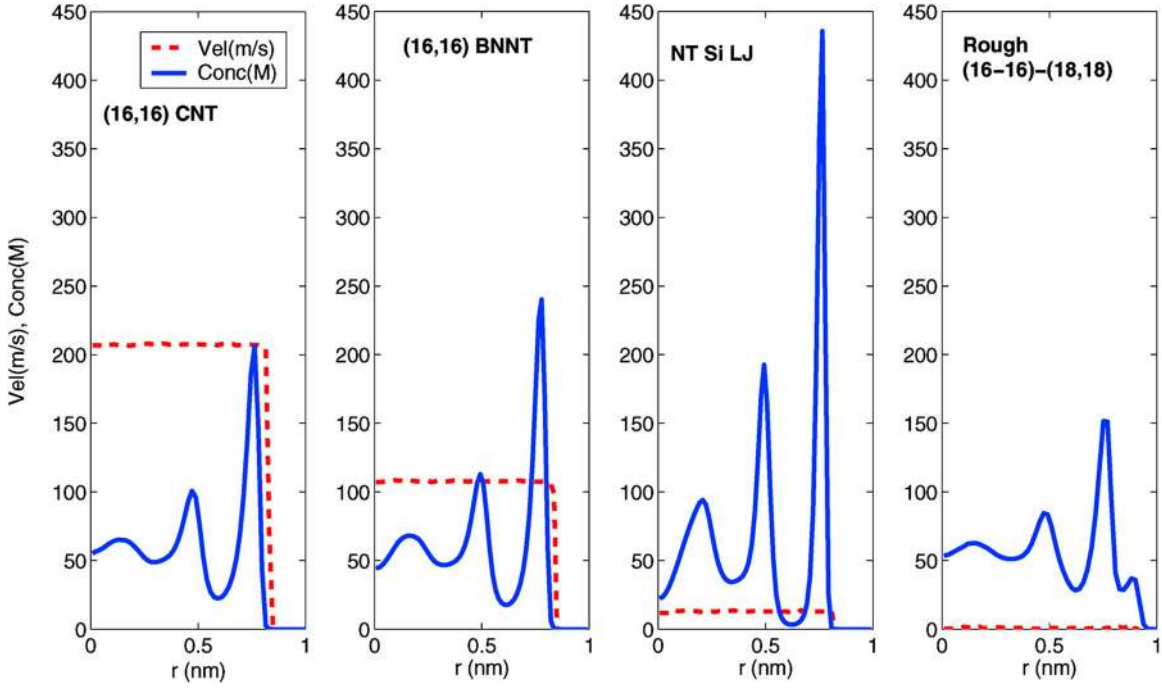

Figure 11. (Colour online) Water concentration in mol/l (M) and velocity profiles in m/s for different systems. For the first three cases, even though the tubes have smooth surfaces, the magnitude of the flow velocities show marked differences. The bulk concentration is 55 M. Reprinted with permission from Joseph et al. [73]. Copyright (2008) American Chemical Society.

non-polar CNTs with a diameter of around 7 nm and length 6.2 nm were simulated. Fluid flow was driven by a hydrostatic pressure difference across all the CNTs. With a gradual increase in surface polarity, the radial dependence of the velocity showed a transition from plug-like to the parabolic flow profile. This was inferred to be due to the enhanced interactions between the water molecules and CNT surface causing resistance to its translation. Further studies were performed to check the flow rate dependence on length in polar CNTs. In non-polar CNTs, the flow rate was found to remain independent of the length, whereas a 10% decrement in the flow rate was observed when the length of the polar CNT was doubled (12.4 nm). This was credited to the increased interactions occurring between the charged surface and polar water molecules. The flow rates were 73% and 63% lower than in pristine nanotubes for polar CNTs of length 6.2 and 12.4 nm, respectively. Finally, MD simulations were carried out in CNTs of length 6.2 and 12.4 nm, having (i) charged functional groups and (ii) higher roughness. In both cases, a decrease in flow rate was reported. The surface roughness induced a turbulent flow inside the tubes, whereas the presence of functional groups in CNTs raised the interaction energy to 1.66 kcal/mol per water molecule (interaction energy is 0.34 kcal/mol for unfunctionalised tubes), which led to a decline in flow rate.

The negligible dependence of flow rate on tube length in non-polar CNTs was explained by Nicholls et al. [14]. They examined the flow velocity, mass flow rate and axial properties of water flowing through a (7,7) CNT with lengths between 2.5 and 50 nm. NEMD simulations were conducted for all the aforementioned lengths of CNTs by applying a constant pressure difference of 200 MPa. The average flow velocity obtained was 14.6 m/s and the average mass flow rate was 3.11×10^{-15} kg/s for all the CNT lengths. The results of the simulation indicated that an increase in length had no remarkable effect on the fluid velocity and mass flow rate. The constant mass flow rate observed was due to the nearly frictionless transport of water through the central 'developed' region of CNT irrespective of the tube length. Though the pressure difference is kept constant, the pressure gradient varies with the tube length which was expected to alter the mass flow rate [12]. However, from the similar flow rates observed in all the tubes, it was inferred that the principal driving force that governs the flow, in this case, is the pressure difference and not the pressure gradient.

The simulation studies discussed above and in general have considered pristine CNTs with no topological defects. Vijayaraghavan et al. [112] investigated the role of geometrical characteristics such as the location and concentration of defects of the SWNTs on confined fluid transport. The simulation model consists of a water-filled CNT system with graphene sheets on either end separated by a distance of 5 nm. Three open-ended armchair CNTs (5,5), (7,7) and (10,10) having the same length (10 nm) were considered for the study. Vacancies (defects) were made either on the graphene sheets (water was drawn inside the tube by the downward movement of graphene sheet) or on the SWNT and the vacancy concentration varied from 6 to 24 defects. It was observed that increasing the number of defects in the graphene sheets reduced the pressure developed within the system. This eventually affects the rapid transport of water through CNTs and brought about a reduction in the number of water molecules passing per unit cross-sectional area in all the SWNTs. The percentage loss of flux relative to the highest vacancy concentration (i.e. 24 defects) was 35.5% for (5,5) CNT while for (10,10) CNT it was 6.7%, suggesting that the transport losses can be minimised by using a higher diameter CNT. Furthermore, the influence of interlayer spacing in double-walled nanotubes (DWNTs) on the transport properties of water was also investigated. Four DWNTs with a uniform outer diameter ((15,15) CNT) but with varying inner diameters (5,5), (7,7) and (10,10) were considered for the study. In DWNT with (10,10) inner CNT, it was observed that the resistive force offered by an increased number of carbon atoms at the entrance region retarded the transport of water molecules compared to the (10,10) SWNT. A higher inter-layer spacing, however, enhanced the efficacy of water transport in DWNTs due to the availability of sufficient space for easy entry of water molecules.

Liu and Patey [113] analysed the water conduction rates through CNTs as influenced by the water models used in atomistic simulations. Three water models: TIP3P, SPC/E and TIP4P/2005, and two CNTs: (8,8) and (9,9) were studied. Water was driven through the tubes under a pressure difference of 220 MPa. For both the tube diameters, the simulations performed using the TIP3P model exhibited the highest flow rate followed by SPC/E and TIP4P/2005. The flow rates with TIP3P were found to be 287 for (8,8) CNT and 492 for (9,9) CNT, which was approximately five times higher when compared to the TIP4P/2005 model. The disparities in the flow rate magnitude were attributed to the distinctive structure and configurations of water formed inside CNTs using different water models. In all the models, water formed two structural configurations which are (i) ring-bound configuration, where hydrogen bonds link the adjacent water molecules in the form of stacked rings comprising of 4–6 entities (i.e. square, pentagonal and hexagonal rings, respectively) and (ii) ring-free configuration. Due to the relatively lower spatial confinement, the percentage of square ring configurations formed inside the (8,8) CNT was the highest (values with the models), whereas in the (9, 9) CNT, pentagonal and hexagonal rings were dominant. However, a higher percentage of ring-free structures formed in (8,8) and (9,9) CNTs with the TIP3P model were found responsible for the faster conduction of water. A similar variation in flow rate with differing water models was also observed in a (6,6) CNT [114]. Here, water forms a one-dimensional single-file chain structure inside the (6,6) CNT for all the water models. Therefore, it was inferred that the difference in flow rate arises not because of the water structural differences but due to the different bulk properties of the water models. Losey et al. [115] also studied the flow of water in CNTs for a variety of water models. They furthermore looked at two types of systems: a CNT connecting two water reservoirs under different pressures (pressure gradient induced flow) and periodic CNTs with constant external field inducing the flow. They found that differences in flow rates due to different water models were significant only in the dual-reservoir systems and attributed this difference to entry/exit effects, whereas no significant model dependencies were found for the periodic CNT systems.

The greater computational expenses incurred for MD simulations to characterise flow through nanochannels in the experimental scales prompted Popadic et al. [116] to study water transport in CNTs using the continuum approach. The finite volume discretisation method was utilised to solve incompressible steady-state Navier–Stokes equations assuming partial-slip boundary conditions. The simulation set up consisted of a collection of CNTs in a membrane each with a radius 1.017 nm and with lengths varying from 3 to 7000 nm. The system comprises of water reservoirs on either side of the membrane. The uniform velocity boundary condition applied to the inlet reservoir kept the flow rate between 0.8 and 10 $\mu m^3 s^{-1}$, whereas, a uniform pressure was maintained at the outlet reservoir. At a given slip length of 63 nm (taken from previous MD simulations) and constant Reynolds number (Re) of 1.4×10^{-3}, the flow rates and corresponding enhancements were calculated for different CNT lengths. A monotonically increasing trend in enhancement was obtained with an increase in length which reached an asymptotic value of 248 for lengths exceeding 2000 nm.

4.3. Theory – continuum model

Myers [117] proposed a theoretical explanation for the large flow enhancement observed in CNTs using continuum hydrodynamics theory. Due to the presence of large non-interacting van der Waals distances in the depletion layer, a bi-viscosity model was considered for the study. In this model, pressure-driven fluid flow in a tube of radius R and length L having a bulk region ($0 \le r \le \alpha$) with viscosity η_1 and an annular region of thickness $\delta(\alpha \le r \le R)$ with viscosity η_2 was considered. The general Navier–Stokes equation was solved by assuming boundary conditions such as no-slip at the wall, symmetry at the tube centre, and continuity of shear stress and velocity at the interface between the fluids (i.e. at $r = \alpha$). Expressions for the flow velocity in the bulk and annular regions (u_1 and u_2), total flow rate (Q) and the flow enhancement (ε) relative to the Hagen–Poiseuille equation are shown in Equations (6), (7) and (8) respectively.

$$u_1 = \frac{p_z}{4\eta_1}\left(r^2 - \alpha^2\right) - \frac{p_z}{4\eta_2}\left(R^2 - \alpha^2\right), \qquad u_2 = \frac{p_z}{4\eta_2}\left(r^2 - R^2\right) \tag{6}$$

$$Q = -\frac{\pi\alpha^4 p_z}{8\eta_1}\left[1 - \frac{2\eta_1}{\eta_2}\left(1 - \frac{R^2}{\alpha^2}\right)\right] - \frac{\pi\alpha^4 p_z}{8\eta_2}\left(1 - \frac{R^2}{\alpha^2}\right)^2 \tag{7}$$

$$\epsilon = \frac{\alpha^4}{R^4} + \frac{\eta_1}{\eta_2}\left(1 - \frac{\alpha^4}{R^4}\right). \tag{8}$$

From the equations, it was deduced that while flow enhancement showed a monotonic increase with decreasing CNT diameter in narrow tubes, the enhancement became independent of the diameter in wider tubes. Equation (8) showed that the enhancement is possible only if viscosity in the annular region is smaller than the bulk viscosity. Myers extracted data from a previous experimental study [108] to validate his proposed model. For a tube radius of 20 nm, the slip length was found to be 35 nm [108]. This was used to calculate the flow enhancement using the slip model given by Equation (3). From Equation (8), where $\epsilon = 8$, $\alpha = 19.3$ nm and R=20 nm, the viscosity in the annular region was found to be 0.018 times the viscosity of water which is nearly equivalent to the viscosity of oxygen, thereby justifying the existence of a depletion region. On comparing Equations (3) and (8), the slip length was deduced as the length-scale related to the size of the depletion region and viscosity ratio. This continuum model is valid only when the channel dimensions are a minimum of 10 times the molecular diameter of the confined fluid.

Mattia et al. [118] utilised the bi-viscosity model to derive a more general expression for the flow enhancement based on solving the Navier–Stokes equation with appropriate boundary conditions. The only difference made in the boundary conditions compared to the Myers study was that instead of using the no-slip boundary condition, the Navier-slip boundary condition was used where all the other boundary conditions remained the same. On integrating the expressions for the velocity profiles in the bulk and annular regions, combining them and comparing with the Hagen–Poiseuille equation, the expression for enhancement as in Equation (9) was established. Here δ is the thickness of the annular region and λ is the slip length. But, being unable to explain the reason behind the magnified flow rate inside CNTs, the Ruckenstein expression for the velocity at the wall was adopted and replaced in terms of slip length (shown by Equation 10), which varies inversely with the work of adhesion (the amount of energy required to move apart water from CNT walls). This was then substituted for slip length in Equation (9). Because of the lower water–CNT interaction energy, an increment in surface diffusion (D_s) and reduction in work of adhesion (W_A) will occur, thus causing flow rate enhancement. The theoretical model is valid for CNTs with diameters greater than 2 nm and an inverse dependence of flow rate enhancement on R^2 was deduced.

$$\epsilon_{\lambda,\delta} = \left(\frac{R-\delta}{R}\right)^4\left(1 - \frac{\mu_1}{\mu_2}\right) + \frac{\mu_1}{\mu_2}\left(1 + \frac{4\lambda}{R}\right) \tag{9}$$

$$\lambda = \frac{2\mu_2 L}{R}\frac{D_s}{W_A}. \tag{10}$$

5. Discussion

Despite flow rates being reported to exceed those predicted by the classical Hagen–Poiseuille equation by 4–5 orders of magnitude, the commercial use of CNT membranes is still limited. The magnitude of flow rate reported in the experimental literature is largely scattered due to the lack of reliable fabrication techniques to manufacture precisely controlled, uniformly distributed, properly aligned CNT structures and also the inaccurate average diameters of the CNT membranes considered for the determination of flow rate. On the other hand, different simulation studies have been able to qualitatively reproduce experimental results, however, no consensus has been reached on the magnitude of flow rates. Both experimental and simulation studies have reported a monotonic decrease in flow rate enhancement with an increase in tube diameter. However,

the extent up to which the confinement effects are crucial for water transport in CNTs is still unclear. From simulation studies, it is expected that for water, flow enhancement reaches the asymptotic behaviour for diameters greater than around 10 nm [75]. Whereas, in experiments enhancement is observed for diameters even up to ≈50 nm [76]. These discrepancies in the flow rates can be attributed mainly to the difference in the simulation parameters used for mimicking the experimental conditions. The choice of simulation details such as the thermostat or the force field can affect the structure and dynamics of nanoconfined water [119,120]. The incongruity of the reported results can impede the advancement of CNTs for numerous practical applications. Shown in Figure 12 are the scattered flow enhancement factors (ϵ) from previously reported results.

The major sources of disparities between simulation and experimental results are discussed below.

5.1. Experiments

(1) *Inaccurate estimation of tube diameter*
The pore density in CNT-based membranes fabricated from conventional methods is extremely high, i.e. $\approx 10^{12}$ nanopores per cm^2. The densely packed CNTs grown on the membrane substrate has a non-uniform diameter distribution. It is, therefore, a common practice to use a mean diameter for the flow rate calculations. A precise determination of the mean diameter and number density of the nanopores in experiments is extremely difficult and could lead to an inaccurate estimation of the flow rate of water through nanotubes. Also, since fluid slip at the CNT walls significantly varies with tube diameter, assuming constant diameter for all tubes in a membrane to determine the flow rate is not accurate.

(2) *Surrounding matrix*
Studies have shown that the underlying substrates can influence the CNT/graphene properties and may in turn influence the confined flow characteristics. The utilisation of different substrate materials (silicon nitride matrix or polystyrene matrix) could be one of the reasons for the disagreement between different experimental results. Thekkethala and Sathian [121] have shown that the presence of substrate influences the interfacial thermal resistance and in turn, the fluid–solid interaction which will influence the fluid flow behaviour. This is further substantiated by the experiment conducted by Xie et al. [122] where they observed a wide distribution of the slip length in graphene nanochannels. The increased attraction between water and polar hydrophillic silica substrate led to a reduction in flow velocity.

(3) *Pristine and imperfect CNTs, surface functionality*
Another challenge that inhibits the large-scale utility of CNTs is their high cost of fabrication. Experimentally, fabricating a perfect defect-free individual carbon nanotube is extremely difficult. The presence of defects in smaller diameter CNTs can cause a significant reduction in the water flow rate [112]. The inferior surface functionality of the CNT also affect its scope for the use in separation and filtration processes. The low reactivity of the inner surface of CNTs for selectivity improvement is also troubling the scientific community. Majumder et al. [107] found that functionalising the tips and core portions of the nanotube can bring about a significant reduction in water flow rates and even the hydration of CNT pores. However, a recent experimental study demonstrated that functionalising the CNT surface with octadecylphosphonic acid shows a significant reduction of salt passage while maintaining the fast transport of water [123].

(4) *Alignment and chirality of CNTs*
A major challenge is the structure-controlled synthesis of CNTs [124], which is critical to implement in applications such as water desalination. A very narrow distribution of nanotube diameters (0.66–0.93 nm) is vital for the selective permeation of water at high flow rates while rejecting the passage of salt ions. Though individual CNTs of diameter as low as 0.4 nm have been manufactured [86], it is still difficult to achieve large-scale production of vertically aligned CNTs of very small pore diameters on a membrane matrix [125,126]. Moreover measuring the tube diameter, controlling the pressure difference to drive the fluid, and finally performing the nanolitre volume experiments are cumbersome procedures that may also lead to scattered data in experiments.

Even subtle differences in the electronic properties of nanochannels can bring about a significant alteration in the slippage of fluid within these confinements [76,127–130]. The atomic structure of a CNT determined by its chirality largely influences its electronic properties [131–135]. The fine alterations in tube chirality determine whether the CNTs are semiconducting or metallic. Apart from this, structural properties such as diameter that greatly affects fluid flow are also dependent on the tube chirality. Therefore, understanding the role of chirality in the dynamics of confined fluids is very important [136]. Although there has been a significant improvement in the manufacturing of CNTs with predefined chirality and dimensions [137–139], the mass fabrication of CNTs with optimal properties remains a major challenge.

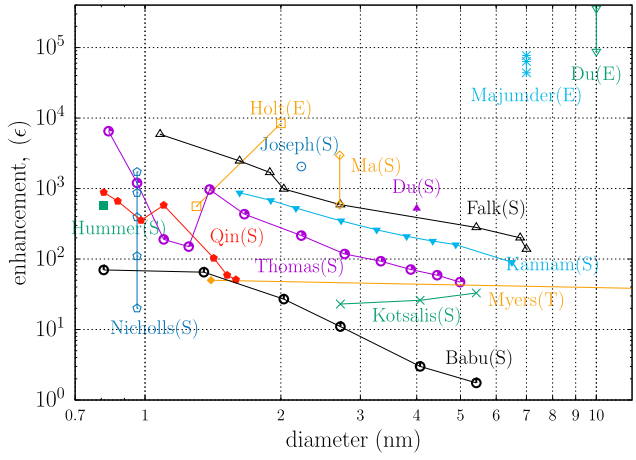

Figure 12. (Colour online) The literature on the flow rate enhancement of water in CNTs of diameter 0.81–44 nm. The author name and method of study, i.e. experiment (E), simulation (S) or theory (T) are denoted in brackets.

Hence it is beneficial to have a better understanding of the role of tube chirality on water transport while conducting experimental studies.

(5) *Fouling of CNT membranes*
Fouling is a critical issue in CNT-based membranes with regard to their higher permeability [140,141]. A higher interaction between the foulants and the hydrophobic CNT surface drastically reduces the water flow rate in CNTs. It was found that the fouling propensity of CNT membranes could potentially be reduced through surface modification using the graft-polymerisation method [142]. However, such modifications could alter the inherent hydrophobicity of these carbonaceous pore membranes, thereby affecting its ultra-fast transport characteristics.

5.2. Simulation

(1) *Non-uniform viscosity and density*
Two of the cardinal factors that determine the rate of fluid flow through nanochannels are (i) the fluid effective shear viscosity and (ii) the slip length at the fluid–solid boundary. The effective shear viscosity is highly dependent on the channel width. It has been observed that channels with a width greater than 3 nm or around 10 fluid molecular diameters have a negligible influence on fluid shear viscosity and an approximately quadratic fluid velocity profile is obtained [143,144]. Conversely, in extremely narrow nanochannels (size of flow domain nearly equal to the size of molecules) the flow density is spatially inhomogeneous, which in turn affects mean transport properties. This likely paves the way for position-dependent transport properties along with non-local response functions. Consequently, shear viscosity across the channel becomes position dependent necessitating the requirement for a non-local viscosity kernel in space for a complete description [145–150]. When such inhomogeneous systems were subjected to MD studies, the effective shear viscosity obtained showed increasing, decreasing and non-monotonic variations with respect to the CNT diameter [10,12,74,151–155]. In most of the previous studies on fluid flow in nanochannels this variation in spatial viscosity, which could affect the effective shear viscosity, was not taken into consideration. This could be one of the factors accountable for the discrepancies observed in slip length and flow rate enhancement, and efforts should be directed towards addressing this challenge [156–161].

(2) *Flexibility of CNTs and thermostat used in simulation*
The dynamics of confined fluids can strongly depend on the method of temperature control employed in MD simulations [162]. The most commonly used approach is by applying the thermostat directly to the fluid with the solid atoms fixed to their lattice sites. Keeping the tube walls rigid while coupling the fluid to a fictitious heat bath is not representative of reality, where heat is exchanged between the wall and the fluid at finite temperature. Sam et al. [163] found that the tube flexibility significantly enhances the fluid flow rate compared to the cases with the rigid tube walls. The flux increment in flexible tubes could be attributed to the transfer of momentum from the excited phonon modes of CNTs to the flowing fluid. The vibrational states of the tube, when coupled with water, results in a fluctuating frictional force between them [164]. The excitation of carbon atoms on the CNT surface may even lead to the reduction of interfacial friction, giving rise to faster flow rates. Future efforts could be directed towards controlling fluid transport by the external actuation of specific vibrational modes within the confining material [165,166]. The choice of the thermostat can also significantly influence the transport characteristics of water in CNTs, with good agreement between the Nosé–Hoover and Berendsen thermostats, while the Langevin thermostat results in different transport behaviours [167].

(3) *Water models*
The water models developed to describe various thermodynamic or structural properties of bulk water can behave very differently in confined situations [168]. Since water models can capture only some aspects of the water accurately, predictions from different models may vary from each other. Studies have shown that water conduction rates through a CNT are strongly model dependent [113–115,169]. In fact, different water models were suggested to be partially responsible for the large variation in reported water flow rates and slip lengths in CNTs. A recent study by Prasad et al. [170] found a difference in the flow rate of up to 84% among various water models. The partial charges, the hydrogen-bond dynamics and the diffusion coefficient of the model were found to influence the water flow rate.

(4) *Cross-species interaction*
The choice of cross-species interaction parameters for modelling the intermolecular interactions are also critical, particularly in sub-nanometre tubes. A minute variation in the water oxygen–carbon interaction strength can result in drying-to-wetting transitions of water [24,171]. With an increase in the values of water–surface interaction energy, the velocity of water at the CNT wall varied from the slip to no-slip condition, causing a drastic reduction in flow enhancement [158]. The water–carbon interaction strength employed in most MD studies was parameterised using experimental contact angle for water droplets. However, an accurate representation of the interactions is still under debate and depends on the empirical parameters used to model the molecular interactions of water and carbon atoms in CNT.

(5) *Electrostatics*
The electrostatic interactions also play a major role in confined water transport. The majority of MD studies modelled CNTs to be electrically neutral (zero partial charge) and calculated only the electrostatic interactions of water. The presence of surface charge in CNTs could significantly alter the flow behaviour of water [172–174]. Moreover, the applicability of the techniques [175–177] used to handle electrostatics in confined flow situations has yet to be examined in detail. For instance, electrostatic interactions include terms that depend on the shape of the

Table 1. Literature on the flow rate enhancement of water in CNTs.

No.	Journal	CNT	Dimensions		Enhancement	Thermostat	H_2O Model	Interaction	Software
			Diameter(nm)	Length				σ_{C-O}, ϵ_{C-O}	
1	Hummer [24] (S)	SW	0.81	1.34 nm	575	B (F)	TIP3P	0.3275, 0.1143	AMBER
2	Kotsalis [72] (S)	SW	2.71–5.42	ns	33-23	B (R)	SPC/E	0.3190, 0.0937	FAST TUBE
3	Majumder [29] (E)	MW	7	34–126 μm	$(43-77)\times10^3$	–	–	–	–
4	Holt [40] (E)	DW	1.3–2.0	2–3 µm	1500–8400	–	–	–	–
5	Thomas [12] (S)	SW	0.83–4.99	(80–12) nm	6500-47	B (R)	TIP5P	0.3190, 0.0936	ns
6	Joseph [73] (S)	SW	2.22	1.42 nm–2 µm	2052	N (R)	SPC/E	0.3190, 0.0937	GROMACS
7	Whitby [108] (E)	MW	44	78 ± 2 µm	20–37	–	–	–	–
8	Falk [30] (S)	SW	0.68–7	ns	5882-138	N (R)	TIP3P	0.3280, 0.1143	LAMMPS
9	Thomas [11] (S)	SW	2.76	1 µm	110	B (R)	TIP5P	0.3190, 0.0936	ns
10	Qin [70] (E)	SW	0.81–1.59	140,280 µm	882-51	–	–	–	–
11	Myers [117] (T)	SW	1.4, 40	78 ± 2 µm	50, 8	–	–	–	–
12	Du [71] (S)	SW	4	5 nm	520	ns	ns	ns, ns	ns
13	Du [71] (E)	DW	10	4000 µm	$(88-360)\times10^3$	–	–	–	–
14	Babu [74] (S)	SW	0.81–5.42	4.795 nm	70-1.8	L (R)	TIP3P	0.3275, 0.1143	LAMMPS
15	Majumder [107] (E)	MW	7	100 µm	$(40-53)\times10^3$	–	–	–	–
16	Majumder [42] (S)	SW	7	(12.4, 6.2) nm	$(39-68)\times10^3$	L (ns)	TIP3P	ns, 0.34	ns
17	Ma [198] (S)	DW	2.7	30 nm	590–2960	N (F)	TIP3P	0.3190, 0.0937	LAMMPS
18	Nicholls [14] (S)	SW	0.96	(2.5–50) nm	20–1720	B (R)	TIP4P	0.3190, 0.0937	mdFoam
19	Su [199] (S)	SW	0.81–2.02	(1.34–9.89) nm	10–400	N (R)	TIP3P	0.3275, 0.1143	GROMACS
20	Kannam [75] (S)	SW	1.62–6.50	(7.37–2.45) nm	870–90	N (F)	SPC/Fw	0.3190, 0.0936	in-house
21	Vijayaraghavan [112](S)	DW	0.94–2.03	10 nm	14.5–4.5	N (R)	FPC	0.3190, 0.0749	ns
22	Thomas [167] (S)	SW	1.4	(1.4, 5, 10) nm	65–325	Various (F)	TIP3P	ns, ns	NAMD

Note: E, S, and T stands for experiment, simulation, and theory respectively. SW, DW and MW stands for single, double and multiwalled nanotubes. Berendsen, Nosé-Hoover and Langevin thermostats are denoted by B, N and L, respectively. F, R indicate flexible and rigid walls. The interaction parameters σ_{C-O} and ϵ_{C-O} are expressed in nm and kcalmol^{-1}. Simulation details not specified in the literature are denoted by ns. The reader is suggested to refer the original papers for details.

system. Electrostatics in the slab geometry are well understood, but less so for other geometries.

(6) *Entrance and exit effects*
Unlike the membranes used in experiments, the majority of simulation studies have considered flow of water through an individual nanotube with periodic boundary conditions along the direction of flow. Such periodic systems are highly effective in studying the fully developed channel flow with minimal computational expenses. However, the effects at the entrance and exit regions of the pores are typically ignored in a periodic system [178]. Joly et al. [179] demonstrated the significant role of entrance effects in the capillary filling of nanopores with water using MD simulations. Further, Walther et al. [180] simulated pressure-driven flow of water in CNT-based membranes with system sizes comparable to the experimental studies. They found that the losses at the entrance and exit regions were dominant for membranes with a thickness less than 3 nm, whereas it could be neglected for membrane thickness of ≈300 nm. The end effects, however, could be significantly reduced by using an hourglass-shaped pore mouth mimicking the aquaporin channels [181–184].

(7) *Large forces for generating Poiseuille flow*
Though considered an effective tool in predicting slip length and fluid velocity at the fluid–solid interface, MD simulation has its limitations. For instance, slip length can be determined using MD by either equilibrium or non-equilibrium methods. Nonequilibrium MD (NEMD) utilises an external force to drive the fluid through the tube, where L_s and the slip velocity (the relative fluid velocity at the wall) can be directly determined from the resultant streaming velocity profile. In high slip systems such as water in a graphitic nanopore, the large slip velocity presents a challenge in predicting the slip length using NEMD simulations. This is because the slip length depends sensitively on the velocity gradient at the surface [185].

Compared to an experimental setup, MD simulations employ smaller systems and shorter simulation times. To obtain a statistically meaningful signal from the relatively small amount of data, much larger driving forces are applied in NEMD simulations than those feasible in experiments. The results obtained from NEMD simulations can be extrapolated down to experimental conditions provided that the fluid response lies in the linear velocity response regime. NEMD simulations need to be performed at multiple external driving forces to verify linear response and to be able to extrapolate the data. Within the limits of the linear regime, L_s remains independent of the driving force as both slip velocity and curvature of the velocity profile exhibit a linear increase with the driving force. However, beyond the linear regime L_s is found to increase rapidly with the driving forces [185].

In equilibrium MD (EMD), an estimation of the slip length can be attained by calculating the interfacial friction using linear response theory [110,186–194]. This is in accordance with the boundary slip expression by Navier (see Equation 1). Another possible method whereby L_s can be determined by EMD simulation is by calculating the relaxation time from the exponential fit of the collective velocity autocorrelation function (VACF) [195–197]. Unlike the NEMD approach, EMD requires only a single simulation for predicting the slip length, and identifying the linear regime is not necessary. Also, EMD methods have been found to be much more accurate and reliable for determining L_s even in high slip systems [190].

Some simulation details, such as forcefield, water models, thermostat, tube dimensions, interaction parameters, enhancement values and so on, are given in Table 1.

6. Conclusion

A sound understanding of the nuances of fluid flow through nanochannels, particularly the flow of water through CNTs, is necessary for exploitation of its potential for application in various fields of science and engineering. Water flow through CNTs is advantageous as it enables both high slip (low energy loss due to friction) and elevated flow rates. The smooth surface, hydrophobicity (weak interaction between water and CNT walls), water OH bond orientation near the tube surface, low activation energy, smooth potential energy landscape, depletion region with low density and reduced viscosity, are all factors that individually or when coupled together help CNTs in attaining their beneficial characteristics. Flow enhancement is highly sensitive to the slip length. This is especially so in high slip conditions such as water in CNTs, and hence flow enhancement measurement using the slip length as a parameter needs to be performed carefully in such systems.

In this review, some of the challenges with regard to water flow through CNTs have been discussed and possible future directions have been suggested that are expected to be beneficial in resolving some of the discrepancies in modelling the slip and enhancing the flow, and aid in improving our understanding of the transport properties of fluids and nanofluidics in general.

Disclosure statement

No potential conflict of interest was reported by the author(s).

ORCID

Alan Sam http://orcid.org/0000-0001-8808-8809
Remco Hartkamp http://orcid.org/0000-0001-8746-8244
Sridhar Kumar Kannam http://orcid.org/0000-0002-8425-5304
Sarith P. Sathian http://orcid.org/0000-0003-2756-7210
Peter J. Daivis http://orcid.org/0000-0001-8454-3341
B. D. Todd http://orcid.org/0000-0003-4683-5719

References

[1] Zhong J, Alibakhshi MA, Xie Q, et al. Exploring anomalous fluid behavior at the nanoscale: direct visualization and quantification via nanofluidic devices. Acc Chem Res. 2020;55(2):347–357.
[2] Eijkel JC, Van Den Berg A. Nanofluidics: what is it and what can we expect from it? Microfluid Nanofluidics. 2005;1(3):249–267.
[3] Bocquet L. Nanofluidics coming of age. Nat Mater. 2020;19(3):254–256.
[4] Agre P. The aquaporin water channels. Proc Am Thorac Soc. 2006;3(1):5–13.
[5] Zeidel ML, Ambudkar SV, Smith BL, et al. Reconstitution of functional water channels in liposomes containing purified red cell chip28 protein. Biochemistry. 1992;31(33):7436–7440.
[6] Radha B, Esfandiar A, Wang F, et al. Molecular transport through capillaries made with atomic-scale precision. Nature. 2016;538 (7624):222–225.
[7] Zhang Z, Wen L, Jiang L. Bioinspired smart asymmetric nanochannel membranes. Chem Soc Rev. 2018;47(2):322–356.
[8] Bocquet L, Charlaix E. Nanofluidics, from bulk to interfaces. Chem Soc Rev. 2010;39(3):1073–1095.
[9] Russo A, Durán-Olivencia MA, Kalliadasis S, et al. Macroscopic relations for microscopic properties at the interface between solid substrates and dense fluids. J Chem Phys. 2019;150(21):214705.
[10] Chen X, Cao G, Han A, et al. Nanoscale fluid transport: size and rate effects. Nano Lett. 2008;8(9):2988–2992.
[11] Thomas JA, McGaughey AJ, Kuter-Arnebeck O. Pressure-driven water flow through carbon nanotubes: insights from molecular dynamics simulation. Int J Thermal Sci. 2010;49(2):281–289.
[12] Thomas JA, McGaughey AJ. Reassessing fast water transport through carbon nanotubes. Nano Lett. 2008;8(9):2788–2793.
[13] Thomas JA, McGaughey AJ. Water flow in carbon nanotubes: transition to subcontinuum transport. Phys Rev Lett. 2009;102(18):184502.
[14] Nicholls WD, Borg MK, Lockerby DA, et al. Water transport through (7,7) carbon nanotubes of different lengths using molecular dynamics. Microfluid Nanofluidics. 2012;12(1-4):257–264.
[15] Xu B, Li Y, Park T, et al. Effect of wall roughness on fluid transport resistance in nanopores. J Chem Phys. 2011;135(14):144703.
[16] Liu B, Wu R, Law AWK, et al. Channel morphology effect on water transport through graphene bilayers. Sci Rep. 2016;6:38583.
[17] Daivis PJ, Todd BD. Challenges in nanofluidics-beyond Navier–Stokes at the molecular scale. Processes. 2018;6(9):144.
[18] Kannam SK, Daivis PJ, Todd B. Modeling slip and flow enhancement of water in carbon nanotubes. MRS Bull. 2017;42(4):283–288.
[19] Prasek J, Drbohlavova J, Chomoucka J, et al. Methods for carbon nanotubes synthesis – review. J Mater Chem. 2011;21(40):15872–15884.
[20] Iijima S. Helical microtubules of graphitic carbon. Nature. 1991;354 (6348):56–58.
[21] Saito R, Dresselhaus G, Dresselhaus MS, et al. Physical properties of carbon nanotubes. Vol. 35. London: Imperial College Press, Imperial College; 1998.
[22] Dresselhaus MS, Dresselhaus G, Eklund P, et al. Carbon nanotubes. Dordrecht: Springer; 2000.
[23] Dresselhaus M. Down the straight and narrow. Nature. 1992;358:195–196.
[24] Hummer G, Rasaiah JC, Noworyta JP. Water conduction through the hydrophobic channel of a carbon nanotube. Nature. 2001;414 (6860):188–190.
[25] Murata K, Mitsuoka K, Hirai T, et al. Structural determinants of water permeation through aquaporin-1. Nature. 2000;407 (6804):599–605.
[26] Sui H, Han BG, Lee JK, et al. Structural basis of water-specific transport through the AQP1 water channel. Nature. 2001;414 (6866):872–878.
[27] Agre P, Borgnia MJ, Yasui M, et al. Discovery of the aquaporins and their impact on basic and clinical physiology. Curr Top Membr. 2001;51:1–38.
[28] Borgnia M, Nielsen S, Engel A, et al. Cellular and molecular biology of the aquaporin water channels. Ann Rev Biochem. 1999;68 (1):425–458.
[29] Majumder M, Chopra N, Andrews R, et al. Nanoscale hydrodynamics: enhanced flow in carbon nanotubes. Nature. 2005;438 (7064):44–44.
[30] Falk K, Sedlmeier F, Joly L, et al. Molecular origin of fast water transport in carbon nanotube membranes: superlubricity versus curvature dependent friction. Nano Lett. 2010;10(10):4067–4073.
[31] Falk K, Sedlmeier F, Joly L, et al. Ultralow liquid/solid friction in carbon nanotubes: comprehensive theory for alcohols, alkanes, omcts, and water. Langmuir. 2012;28(40):14261–14272.
[32] Kalra A, Garde S, Hummer G. Osmotic water transport through carbon nanotube membranes. Proc Natl Acad Sci. 2003;100 (18):10175–10180.
[33] Kosa SA, Al-Zhrani G, Salam MA. Removal of heavy metals from aqueous solutions by multi-walled carbon nanotubes modified with 8-hydroxyquinoline. Chem Eng J. 2012;181–182:159–168.
[34] Salam MA. Coating carbon nanotubes with crystalline manganese dioxide nanoparticles and their application for lead ions removal from model and real water. Colloids Surf A. 2013;419:69–79.
[35] Upadhyayula VK, Deng S, Mitchell MC, et al. Application of carbon nanotube technology for removal of contaminants in drinking water: a review. Sci Total Environ. 2009;408(1):1–13.
[36] Mostafavi S, Mehrnia M, Rashidi A. Preparation of nanofilter from carbon nanotubes for application in virus removal from water. Desalination. 2009;238(1–3):271–280.

[37] Fornasiero F, Park HG, Holt JK, et al. Ion exclusion by sub-2-nm carbon nanotube pores. Proc Natl Acad Sci. 2008;105(45):17250–17255.

[38] Vatanpour V, Madaeni SS, Moradian R, et al. Fabrication and characterization of novel antifouling nanofiltration membrane prepared from oxidized multiwalled carbon nanotube/polyethersulfone nanocomposite. J Membr Sci. 2011;375(1–2):284–294.

[39] Ghosh S, Sood A, Kumar N. Carbon nanotube flow sensors. Science. 2003;299(5609):1042–1044.

[40] Holt JK, Park HG, Wang Y, et al. Fast mass transport through sub-2-nanometer carbon nanotubes. Science. 2006;312(5776):1034–1037.

[41] Corry B. Designing carbon nanotube membranes for efficient water desalination. J Phys Chem B. 2008;112(5):1427–1434.

[42] Majumder M, Corry B. Anomalous decline of water transport in covalently modified carbon nanotube membranes. Chem Commun. 2011;47(27):7683–7685.

[43] Goh P, Ismail A, Ng B. Carbon nanotubes for desalination: performance evaluation and current hurdles. Desalination. 2013;308:2–14.

[44] Semiat R. Energy issues in desalination processes. Environ Sci Technol. 2008;42(22):8193–8201.

[45] Elimelech M, Phillip WA. The future of seawater desalination: energy, technology, and the environment. Science. 2011;333(6043):712–717.

[46] Fritzmann C, Löwenberg J, Wintgens T, et al. State-of-the-art of reverse osmosis desalination. Desalination. 2007;216(1–3):1–76.

[47] Sablani S, Goosen M, Al-Belushi R, et al. Concentration polarization in ultrafiltration and reverse osmosis: a critical review. Desalination. 2001;141(3):269–289.

[48] Maskan F, Wiley DE, Johnston LP, et al. Optimal design of reverse osmosis module networks. AIChE J. 2000;46(5):946–954.

[49] Han Y, Xu Z, Gao C. Ultrathin graphene nanofiltration membrane for water purification. Adv Funct Mater. 2013;23(29):3693–3700.

[50] Wong SS, Joselevich E, Woolley AT, et al. Covalently functionalized nanotubes as nanometre-sized probes in chemistry and biology. Nature. 1998;394(6688):52–55.

[51] Gordillo M, Martı J. Hydrogen bond structure of liquid water confined in nanotubes. Chem Phys Lett. 2000;329(5–6):341–345.

[52] Koga K, Gao G, Tanaka H, et al. Formation of ordered ice nanotubes inside carbon nanotubes. Nature. 2001;412(6849):802–805.

[53] Marti J, Gordillo M. Temperature effects on the static and dynamic properties of liquid water inside nanotubes. Phys Rev E. 2001;64(2):021504.

[54] Walther JH, Jaffe R, Halicioglu T, et al. Carbon nanotubes in water: structural characteristics and energetics. J Phys Chem B. 2001;105(41):9980–9987.

[55] Werder T, Walther JH, Jaffe RL, et al. Molecular dynamics simulation of contact angles of water droplets in carbon nanotubes. Nano Lett. 2001;1(12):697–702.

[56] Noon WH, Ausman KD, Smalley RE, et al. Helical ice-sheets inside carbon nanotubes in the physiological condition. Chem Phys Lett. 2002;355(5–6):445–448.

[57] Pascal TA, Goddard WA, Jung Y. Entropy and the driving force for the filling of carbon nanotubes with water. Proc Natl Acad Sci. 2011;108(29):11794–11798.

[58] Jorgensen WL, Madura JD. Temperature and size dependence for monte carlo simulations of TIP4P water. Mol Phys. 1985;56(6):1381–1392.

[59] Prada-Gracia D, Shevchuk R, Rao F. The quest for self-consistency in hydrogen bond definitions. J Chem Phys. 2013;139(8):084501.

[60] Hartkamp R, Coasne B. Structure and transport of aqueous electrolytes: from simple halides to radionuclide ions. J Chem Phys. 2014;141(12):124508.

[61] Berezhkovskii A, Hummer G. Single-file transport of water molecules through a carbon nanotube. Phys Rev Lett. 2002;89(6):064503.

[62] Hummer G. Water, proton, and ion transport: from nanotubes to proteins. Mol Phys. 2007;105(2-3):201–207.

[63] Cambré S, Schoeters B, Luyckx S, et al. Experimental observation of single-file water filling of thin single-wall carbon nanotubes down to chiral index (5,3). Phys Rev Lett. 2010;104(20):207401.

[64] Borg MK, Lockerby DA, Ritos K, et al. Multiscale simulation of water flow through laboratory-scale nanotube membranes. J Membr Sci. 2018;567:115–126.

[65] Striolo A, Michaelides A, Joly L. The carbon-water interface: modeling challenges and opportunities for the water-energy nexus. Ann Rev Chem Biomol Eng. 2016;7:533–556.

[66] Biedermann F, Nau WM, Schneider HJ. The hydrophobic effect revisited-studies with supramolecular complexes imply high-energy water as a noncovalent driving force. Angew Chem Int Ed. 2014;53(42):11158–11171.

[67] Sam A, Hartkamp R, Kannam SK, et al. Prediction of fluid slip in cylindrical nanopores using equilibrium molecular simulations. Nanotechnology. 2018;29(48):485404.

[68] Navier C. Mémoire sur les lois du mouvement des fluides. Mém Acad Sci Inst France. 1823;6:389–440.

[69] Sam A, Prasad V, Sathian SP. Water flow in carbon nanotubes: the role of tube chirality. Phys Chem Chem Phys. 2019;21(12):6566–6573.

[70] Qin X, Yuan Q, Zhao Y, et al. Measurement of the rate of water translocation through carbon nanotubes. Nano Lett. 2011;11(5):2173–2177.

[71] Du F, Qu L, Xia Z, et al. Membranes of vertically aligned superlong carbon nanotubes. Langmuir. 2011;27(13):8437–8443.

[72] Kotsalis E, Walther J, Koumoutsakos P. Multiphase water flow inside carbon nanotubes. Int J Multiphase Flow. 2004;30(7–8):995–1010.

[73] Joseph S, Aluru N. Why are carbon nanotubes fast transporters of water? Nano Lett. 2008;8(2):452–458.

[74] Babu JS, Sathian SP. The role of activation energy and reduced viscosity on the enhancement of water flow through carbon nanotubes. J Chem Phys. 2011;134(19):194509.

[75] Kannam SK, Todd B, Hansen JS, et al. How fast does water flow in carbon nanotubes? J Chem Phys. 2013;138(9):094701.

[76] Secchi E, Marbach S, Niguès A, et al. Massive radius-dependent flow slippage in carbon nanotubes. Nature. 2016;537(7619):210–213.

[77] Govind Rajan A, Strano MS, Blankschtein D. Liquids with lower wettability can exhibit higher friction on hexagonal boron nitride: the intriguing role of solid–liquid electrostatic interactions. Nano Lett. 2019;19(3):1539–1551.

[78] Siria A, Bocquet ML, Bocquet L. New avenues for the large-scale harvesting of blue energy. Nat Rev Chem. 2017;1(11):1–10.

[79] Iijima S, Ajayan P, Ichihashi T. Growth model for carbon nanotubes. Phys Rev Lett. 1992;69(21):3100.

[80] Ebbesen T, Ajayan P. Large-scale synthesis of carbon nanotubes. Nature. 1992;358(6383):220–222.

[81] Iijima S, Ichihashi T. Single-shell carbon nanotubes of 1-nm diameter. 1993.

[82] Bethune D, Klang C, De Vries M, et al. Cobalt-catalysed growth of carbon nanotubes with single-atomic-layer walls. 1993.

[83] Liu C, Cong H, Li F, et al. Semi-continuous synthesis of single-walled carbon nanotubes by a hydrogen arc discharge method. Carbon. 1999;37(11):1865–1868.

[84] Antisari MV, Marazzi R, Krsmanovic R. Synthesis of multiwall carbon nanotubes by electric arc discharge in liquid environments. Carbon. 2003;41(12):2393–2401.

[85] Zhu Hw, Jiang B, Xu Cl, et al. Synthesis of high quality single-walled carbon nanotube silks by the arc discharge technique. J Phys Chem B. 2003;107(27):6514–6518.

[86] Li H, Guan L, Shi Z, et al. Direct synthesis of high purity single-walled carbon nanotube fibers by arc discharge. J Phys Chem B. 2004;108(15):4573–4575.

[87] Journet C, Maser W, Bernier P, et al. Large-scale production of single-walled carbon nanotubes by the electric-arc technique. Nature. 1997;388(6644):756–758.

[88] Thess A, Lee R, Nikolaev P, et al. Crystalline ropes of metallic carbon nanotubes. Science. 1996;273(5274):483.

[89] Braidy N, El Khakani M, Botton G. Carbon nanotubular structures synthesis by means of ultraviolet laser ablation. J Mater Res. 2002;17(09):2189–2192.
[90] Takahashi S, Ikuno T, Oyama T, et al. Synthesis and characterization of carbon nanotubes grown on carbon particles by using high vacuum laser ablation. (Japanese title: Kō shinkū rēzāaburēshon o shiyō shite tanso ryūshi-jō ni seichōshita kābon'nanochūbu no gōsei to tokusei hyōka). J Vac Soc Jpn. 2002;45:609–612.
[91] Vander Wal R, Berger G, Ticich T. Carbon nanotube synthesis in a flame using laser ablation for in situ catalyst generation. Appl Phys A. 2003;77(7):885–889.
[92] José-Yacamán M, Miki-Yoshida M, Rendon L, et al. Catalytic growth of carbon microtubules with fullerene structure. Appl Phys Lett. 1993;62(2):202–204.
[93] Li W, Xie S, Qian L, et al. Large-scale synthesis of aligned carbon nanotubes. Science. 1996;274(5293):1701.
[94] Qin L. Cvd synthesis of carbon nanotubes. J Mater Sci Lett. 1997;16 (6):457–459.
[95] Choi YC, Bae DJ, Lee YH, et al. Growth of carbon nanotubes by microwave plasma-enhanced chemical vapor deposition at low temperature. J Vac Sci Technol A. 2000;18(4):1864–1868.
[96] Varadan VK, Xie J. Large-scale synthesis of multi-walled carbon nanotubes by microwave CVD. Smart Mater Struct. 2002;11(4):610.
[97] Chatterjee A, Sharon M, Banerjee R, et al. CVD synthesis of carbon nanotubes using a finely dispersed cobalt catalyst and their use in double layer electrochemical capacitors. Electrochim Acta. 2003;48(23):3439–3446.
[98] Park D, Kim YH, Lee JK. Synthesis of carbon nanotubes on metallic substrates by a sequential combination of pecvd and thermal CVD. Carbon. 2003;41(5):1025–1029.
[99] Chaisitsak S, Yamada A, Konagai M. Hot filament enhanced CVD synthesis of carbon nanotubes by using a carbon filament. Diam Relat Mater. 2004;13(3):438–444.
[100] Seidel R, Duesberg GS, Unger E, et al. Chemical vapor deposition growth of single-walled carbon nanotubes at 600°C and a simple growth model. J Phys Chem B. 2004;108(6):1888–1893.
[101] Das R, Ali ME, Hamid SBA, et al. Carbon nanotube membranes for water purification: a bright future in water desalination. Desalination. 2014;336:97–109.
[102] Li S, Liao G, Liu Z, et al. Enhanced water flux in vertically aligned carbon nanotube arrays and polyethersulfone composite membranes. J Mater Chem A. 2014;2(31):12171–12176.
[103] Yamada T, Namai T, Hata K, et al. Size-selective growth of double-walled carbon nanotube forests from engineered iron catalysts. Nat Nanotechnol. 2006;1(2):131–136.
[104] Hiramatsu M, Deguchi T, Nagao H, et al. Aligned growth of single-walled and double-walled carbon nanotube films by control of catalyst preparation. Jap J Appl Phys. 2007;46(4L):L303.
[105] Hinds BJ, Chopra N, Rantell T, et al. Aligned multiwalled carbon nanotube membranes. Science. 2004;303(5654):62–65.
[106] Holt JK, Noy A, Huser T, et al. Fabrication of a carbon nanotube-embedded silicon nitride membrane for studies of nanometer-scale mass transport. Nano Lett. 2004;4(11):2245–2250.
[107] Majumder M, Chopra N, Hinds BJ. Mass transport through carbon nanotube membranes in three different regimes: ionic diffusion and gas and liquid flow. ACS Nano. 2011;5(5):3867–3877.
[108] Whitby M, Cagnon L, Thanou M, et al. Enhanced fluid flow through nanoscale carbon pipes. Nano Lett. 2008;8(9):2632–2637.
[109] Figueras L, Faraudo J. Competition between hydrogen bonding and electric field in single-file transport of water in carbon nanotubes. Mol Simul. 2012;38(1):23–25.
[110] Hansen JS, Todd B, Daivis PJ. Prediction of fluid velocity slip at solid surfaces. Phys Rev E. 2011;84(1):016313.
[111] Liu YC, Shen JW, Gubbins KE, et al. Diffusion dynamics of water controlled by topology of potential energy surface inside carbon nanotubes. Phys Rev B. 2008;77(12):125438.
[112] Vijayaraghavan V, Wong C. Transport characteristics of water molecules in carbon nanotubes investigated by using molecular dynamics simulation. Comput Mater Sci. 2014;89:36–44.
[113] Liu L, Patey G. Simulations of water transport through carbon nanotubes: how different water models influence the conduction rate. J Chem Phys. 2014;141(18):18C518.
[114] Liu L, Patey G. Simulated conduction rates of water through a (6,6) carbon nanotube strongly depend on bulk properties of the model employed. J Chem Phys. 2016;144(18):184502.
[115] Losey J, Kannam SK, Todd B, et al. Flow of water through carbon nanotubes predicted by different atomistic water models. J Chem Phys. 2019;150(19):194501.
[116] Popadić A, Walther JH, Koumoutsakos P, et al. Continuum simulations of water flow in carbon nanotube membranes. New J Phys. 2014;16(8):082001.
[117] Myers TG. Why are slip lengths so large in carbon nanotubes? Microfluid Nanofluidics. 2011;10(5):1141–1145.
[118] Mattia D, Calabrò F. Explaining high flow rate of water in carbon nanotubes via solid–liquid molecular interactions. Microfluid Nanofluidics. 2012;13(1):125–130.
[119] Alexiadis A, Kassinos S. Molecular simulation of water in carbon nanotubes. Chem Rev. 2008;108(12):5014–5034.
[120] Markesteijn A, Hartkamp R, Luding S, et al. A comparison of the value of viscosity for several water models using poiseuille flow in a nano-channel. J Chem Phys. 2012;136(13):134104.
[121] Thekkethala JF, Sathian SP. The effect of graphene layers on interfacial thermal resistance in composite nanochannels with flow. Microfluid Nanofluidics. 2015;18(4):637–648.
[122] Xie Q, Alibakhshi MA, Jiao S, et al. Fast water transport in graphene nanofluidic channels. Nat Nanotechnol. 2018;13(3):238–245.
[123] Lokesh M, Youn SK, Park HG. Osmotic transport across surface functionalized carbon nanotube membrane. Nano Lett. 2018;18 (11):6679–6685.
[124] Rao R, Pint CL, Islam AE, et al. Carbon nanotubes and related nanomaterials: critical advances and challenges for synthesis toward mainstream commercial applications. ACS Nano. 2018;12 (12):11756–11784.
[125] Kim S, Jinschek JR, Chen H, et al. Scalable fabrication of carbon nanotube/polymer nanocomposite membranes for high flux gas transport. Nano Lett. 2007;7(9):2806–2811.
[126] Yu M, Funke HH, Falconer JL, et al. High density, vertically-aligned carbon nanotube membranes. Nano Lett. 2008;9(1):225–229.
[127] Tocci G, Joly L, Michaelides A. Friction of water on graphene and hexagonal boron nitride from ab initio methods: very different slippage despite very similar interface structures. Nano Lett. 2014;14 (12):6872–6877.
[128] Sokoloff J. Enhancement of the water flow velocity through carbon nanotubes resulting from the radius dependence of the friction due to electron excitations. Phys Rev E. 2018;97(3):033107.
[129] Michaelides A. Nanoscience: slippery when narrow. Nature. 2016;537(7619):171–172.
[130] Velioğlu S, Karahan HE, Goh K, et al. Metallicity-dependent ultrafast water transport in carbon nanotubes. Small. 2020;1907575. https://doi.org/10.1002/smll.201907575
[131] Saito R, Fujita M, Dresselhaus G, et al. Electronic structure of chiral graphene tubules. Appl Phys Lett. 1992;60(18):2204–2206.
[132] Louie SG. Electronic properties, junctions, and defects of carbon nanotubes. In: Carbon nanotubes. Berlin: Springer; 2001. p. 113–145.
[133] Tans SJ, Devoret MH, Dai H, et al. Individual single-wall carbon nanotubes as quantum wires. Nature. 1997;386(6624):474.
[134] Mintmire JW, Dunlap B, White C. Are fullerene tubules metallic? Phys Rev Lett. 1992;68(5):631.
[135] Hamada N, Sawada Si, Oshiyama A. New one-dimensional conductors: graphitic microtubules. Phys Rev Lett. 1992;68 (10):1579.
[136] Goh K, Chen Y. Controlling water transport in carbon nanotubes. Nano Today. 2017;14:13–15.
[137] Liu J, Wang C, Tu X, et al. Chirality-controlled synthesis of single-wall carbon nanotubes using vapour-phase epitaxy. Nat Commun. 2012;3:1199.
[138] Yang F, Wang X, Zhang D, et al. Chirality-specific growth of single-walled carbon nanotubes on solid alloy catalysts. Nature. 2014;510 (7506):522.

[139] Liu B, Liu J, Tu X, et al. Chirality-dependent vapor-phase epitaxial growth and termination of single-wall carbon nanotubes. Nano Lett. 2013;13(9):4416–4421.
[140] Gu M, Vegas AJ, Anderson DG, et al. Combinatorial synthesis with high throughput discovery of protein-resistant membrane surfaces. Biomaterials. 2013;34(26):6133–6138.
[141] Imbrogno J, Williams MD, Belfort G. A new combinatorial method for synthesizing, screening, and discovering antifouling surface chemistries. ACS Appl Mater Interfaces. 2015;7(4):2385–2392.
[142] Park SM, Jung J, Lee S, et al. Fouling and rejection behavior of carbon nanotube membranes. Desalination. 2014;343:180–186.
[143] Travis KP, Todd B, Evans DJ. Departure from Navier–Stokes hydrodynamics in confined liquids. Phys Rev E. 1997;55(4):4288.
[144] Travis KP, Gubbins KE. Poiseuille flow of Lennard–Jones fluids in narrow slit pores. J Chem Phys. 2000;112(4):1984–1994.
[145] Todd B, Hansen J. Nonlocal viscous transport and the effect on fluid stress. Phys Rev E. 2008;78(5):051202.
[146] Todd B, Hansen J, Daivis PJ. Nonlocal shear stress for homogeneous fluids. Phys Rev Lett. 2008;100(19):195901.
[147] Dalton BA, Daivis PJ, Hansen JS, et al. Effects of nanoscale density inhomogeneities on shearing fluids. Phys Rev E. 2013;88(5):052143.
[148] Glavatskiy KS, Dalton BA, Daivis PJ, et al. Nonlocal response functions for predicting shear flow of strongly inhomogeneous fluids. I. Sinusoidally driven shear and sinusoidally driven inhomogeneity. Phys Rev E. 2015;91(6):062132.
[149] Dalton BA, Glavatskiy KS, Daivis PJ, et al. Nonlocal response functions for predicting shear flow of strongly inhomogeneous fluids. II. Sinusoidally driven shear and multisinusoidal inhomogeneity. Phys Rev E. 2015;92(1):012108.
[150] Dalton BA, Glavatskiy KS, Daivis PJ, et al. Linear and nonlinear density response functions for a simple atomic fluid. J Chem Phys. 2013;139(4):044510.
[151] Liu Y, Wang Q. Transport behavior of water confined in carbon nanotubes. Phys Rev B. 2005;72(8):085420.
[152] Liu Y, Wang Q, Wu T, et al. Fluid structure and transport properties of water inside carbon nanotubes. J Chem Phys. 2005;123(23):234701.
[153] Ye H, Zhang H, Zhang Z, et al. Size and temperature effects on the viscosity of water inside carbon nanotubes. Nanoscale Res Lett. 2011;6(1):1–5.
[154] Zhang H, Ye H, Zheng Y, et al. Prediction of the viscosity of water confined in carbon nanotubes. Microfluid Nanofluidics. 2011;10(2):403–414.
[155] Wu K, Chen Z, Li J, et al. Wettability effect on nanoconfined water flow. Proc Natl Acad Sci. 2017;114(13):3358–3363.
[156] Neek-Amal M, Peeters FM, Grigorieva IV, et al. Commensurability effects in viscosity of nanoconfined water. ACS Nano. 2016;10(3):3685–3692.
[157] Wang Y, Xu J, Wang S, et al. Quantitative relationship between fluid inhomogeneities and flow enhancement in nanotubes. Nanoscale. 2017;9(20):6777–6782.
[158] Shaat M, Zheng Y. Fluidity and phase transitions of water in hydrophobic and hydrophilic nanotubes. Sci Rep. 2019;9(1):5689.
[159] Feng D, Li X, Wang X, et al. Capillary filling of confined water in nanopores: coupling the increased viscosity and slippage. Chem Eng Sci. 2018;186:228–239.
[160] Camargo D, de la Torre JA, Duque-Zumajo D, et al. Nanoscale hydrodynamics near solids. J Chem Phys. 2018;148(6):064107.
[161] Camargo D, de la Torre JA, Delgado-Buscalioni R, et al. Boundary conditions derived from a microscopic theory of hydrodynamics near solids. J Chem Phys. 2019;150(14):144104.
[162] Bernardi S, Todd B, Searles DJ. Thermostating highly confined fluids. J Chem Phys. 2010;132(24):244706.
[163] Sam A, Kannam SK, Hartkamp R, et al. Water flow in carbon nanotubes: the effect of tube flexibility and thermostat. J Chem Phys. 2017;146(23):234701.
[164] Ma M, Grey F, Shen L, et al. Water transport inside carbon nanotubes mediated by phonon-induced oscillating friction. Nat Nanotechnol. 2015;10(8):692.
[165] Cao W, Wang J, Ma M. Carbon nanostructure based mechano-nanofluidics. J Micromech Microeng. 2018;28(3):033001.
[166] Cao W, Wang J, Ma M. Water diffusion in wiggling graphene membranes. J Phys Chem Lett. 2019;10(22):7251–7258.
[167] Thomas M, Corry B. Thermostat choice significantly influences water flow rates in molecular dynamics studies of carbon nanotubes. Microfluid Nanofluidics. 2015;18(1):41–47.
[168] Vega C, Abascal JL. Simulating water with rigid non-polarizable models: a general perspective. Phys Chem Chem Phys. 2011;13(44):19663–19688.
[169] Celebi AT, Nguyen CT, Hartkamp R, et al. The role of water models on the prediction of slip length of water in graphene nanochannels. J Chem Phys. 2019;151(17):174705.
[170] Prasad V, Kannam SK, Hartkamp R, et al. Water desalination using graphene nanopores: influence of the water models used in simulations. Phys Chem Chem Phys. 2018;20(23):16005–16011.
[171] Melillo M, Zhu F, Snyder MA, et al. Water transport through nanotubes with varying interaction strength between tube wall and water. J Phys Chem Lett. 2011;2(23):2978–2983.
[172] Shen C, Guo W. Manipulation of long-range water ordering in less confined nanotubes. J Phys Chem C. 2019;123(15):10101–10106.
[173] Xie Y, Fu L, Joly L. Liquid–solid slip on charged walls: dramatic impact of charge distribution. Preprint 2020. arXiv:200202444.
[174] Wang C, Yang H, Wang X, et al. Unexpected large impact of small charges on surface frictions with similar wetting properties. Commun Chem. 2020;3(1):1–7.
[175] Wolf D, Keblinski P, Phillpot S, et al. Exact method for the simulation of Coulombic systems by spherically truncated, pairwise r-1 summation. J Chem Phys. 1999;110(17):8254–8282.
[176] Ewald PP. Ewald summation. Ann Phys. 1921;369:253.
[177] Yeh IC, Berkowitz ML. Ewald summation for systems with slab geometry. J Chem Phys. 1999;111(7):3155–3162.
[178] Sisan TB, Lichter S. The end of nanochannels. Microfluid Nanofluidics. 2011;11(6):787–791.
[179] Joly L. Capillary filling with giant liquid/solid slip: dynamics of water uptake by carbon nanotubes. J Chem Phys. 2011;135(21):214705.
[180] Walther JH, Ritos K, Cruz-Chu ER, et al. Barriers to superfast water transport in carbon nanotube membranes. Nano Lett. 2013;13(5):1910–1914.
[181] Gravelle S, Joly L, Detcheverry F, et al. Optimizing water permeability through the hourglass shape of aquaporins. Proc Natl Acad Sci. 2013;110(41):16367–16372.
[182] Gravelle S, Joly L, Ybert C, et al. Large permeabilities of hourglass nanopores: from hydrodynamics to single file transport. J Chem Phys. 2014;141(18):18C526.
[183] Tang D, Yoo YE, Kim D. Molecular dynamics simulations on water permeation through hourglass-shaped nanopores with varying pore geometry. Chem Phys. 2015;453:13–19.
[184] Zhang X, Zhou W, Xu F, et al. Resistance of water transport in carbon nanotube membranes. Nanoscale. 2018;10(27):13242–13249.
[185] Kannam SK, Todd B, Hansen JS, et al. Slip length of water on graphene: limitations of non-equilibrium molecular dynamics simulations. J Chem Phys. 2012;136(2):024705.
[186] Bocquet L, Barrat JL. Hydrodynamic boundary conditions, correlation functions, and kubo relations for confined fluids. Phys Rev E. 1994;49(4):3079.
[187] Sokhan V, Nicholson D, Quirke N. Fluid flow in nanopores: an examination of hydrodynamic boundary conditions. J Chem Phys. 2001;115(8):3878–3887.
[188] Sokhan VP, Nicholson D, Quirke N. Fluid flow in nanopores: accurate boundary conditions for carbon nanotubes. J Chem Phys. 2002;117(18):8531–8539.
[189] Chen S, Wang H, Qian T, et al. Determining hydrodynamic boundary conditions from equilibrium fluctuations. Phys Rev E. 2015;92(4):043007.
[190] Kannam SK, Todd B, Hansen JS, et al. Slip flow in graphene nanochannels. J Chem Phys. 2011;135(14):144701.

[191] Kannam SK, Todd B, Hansen JS, et al. Interfacial slip friction at a fluid-solid cylindrical boundary. J Chem Phys. 2012;136(24):244704.
[192] Oga H, Yamaguchi Y, Omori T, et al. Green-kubo measurement of liquid-solid friction in finite-size systems. J Chem Phys. 2019;151 (5):054502.
[193] Petravic J, Harrowell P. On the equilibrium calculation of the friction coefficient for liquid slip against a wall. J Chem Phys. 2007;127 (17):174706.
[194] Huang K, Szlufarska I. Green-kubo relation for friction at liquid-solid interfaces. Phys Rev E. 2014;89(3):032119.
[195] Sokhan VP, Quirke N. Slip coefficient in nanoscale pore flow. Phys Rev E. 2008;78(1):015301.
[196] Sokhan VP, Quirke N. Interfacial friction and collective diffusion in nanopores. Mol Simul. 2004;30(4):217–224.
[197] Groombridge M, Schneemilch M, Quirke N. Slip boundaries in nanopores. Mol Simul. 2011;37(12):1023–1030.
[198] Ma MD, Shen L, Sheridan J, et al. Friction of water slipping in carbon nanotubes. Phys Rev E. 2011;83(3):036316.
[199] Su J, Guo H. Effect of nanochannel dimension on the transport of water molecules. J Phys Chem B. 2012;116(20):5925–5932.